
Angularity in Higgs boson decays via $H \rightarrow gg$ at NNLL' accuracy^{*}

Jiawei Zhu (朱佳伟)¹, Yujin Song (宋昱锦)¹, Jun Gao (高俊)², Daekyoung Kang^{1,3}, Tanmay Maji⁴

¹ Key Laboratory of Nuclear Physics and Ion-beam Application (MOE) and Institute of Modern Physics,
Fudan University, Shanghai 200433, China

²School of Physics and Astronomy, Shanghai Key Laboratory for Particle Physics and Cosmology, and Key Laboratory for Particle
Astrophysics and Cosmology (MOE), Shanghai Jiao Tong University, Shanghai 200240, China

³Department of Physics, Korea University, Seoul 02841, Korea

⁴Department of Physics, National Institute of Technology, Kurukshetra, Haryana, 136 119, India

Abstract: We present improved predictions of a class of event-shape distributions called angularity for a contribution from an effective operator $H \rightarrow gg$ in Higgs hadronic decay that suffers from large perturbative uncertainties. In the frame of Soft-Collinear Effective Theory, logarithmic terms of the distribution are resummed at NNLL' accuracy, for which 2-loop constant of gluon-jet function for angularity is independently determined by a fit to fixed-order distribution at NLO corresponding to $\mathcal{O}(\alpha_s^2)$ relative to the Born rate. Our determination shows reasonable agreement with the value in a thesis recently released. In the fit, we use an asymptotic form with a fractional power conjectured from recoil corrections at one-loop order and it improves the accuracy of determination in positive values of angularity parameter a . The resummed distribution is matched to the NLO fixed-order results to make our predictions valid at all angularity values. We also discuss the first moment and subtracted moment of angularity as a function of a that allow to extract information on leading and subleading nonperturbative corrections associated with gluons.

Key words: Higgs decay; Soft-collinear effective theory; angularity; resummation

1 Introduction

Since the experimental discovery of Higgs boson, the final piece of the Standard Model, the continuous operation of the Large Hadron Collider (LHC), the ATLAS and CMS experiments [1, 2] have shown great success on refined study of the Higgs boson, for example, determination of the Higgs couplings with top quarks [3, 4] and bottom quarks [5, 6]. At the LHC, the huge background restricts the accuracy of measurements on the Higgs signal strength not to below 5% [7] and also very difficult to probe Yukawa couplings of the light fermions of first two generations [8–16]. The sensitivity to Higgs self-interactions is also weak [17–20]. There are future experimental proposals to probe its properties and the rare decay modes of Higgs boson with higher accuracy, e.g., the International Linear Collider [21] and the Circular Electron-Positron Collider (CEPC) [22], CLIC [23], FCC- ee [24]. In the future electron-positrons colliders, most of the possible decay channels of Higgs boson can be studied with high precision and total width of the Higgs boson can be reconstructed in a model independent way. Hadronic decay of Higgs boson, where the final state

consists of hadrons, is one of dominant decay modes that will be extensively studied in the Higgs factories. The hadronic decay is initiated by quarks and gluons. The former is induced by Yukawa-coupling operator $H \rightarrow q\bar{q}$ and the latter is by an effective gluon operator $H \rightarrow gg$ through the top-quark loop, which we refer to as the quark channel and gluon channel, respectively. Event shapes are the classic observables designed to describe the geometry of final hadrons. An application of event shapes for Higgs decay is discussed in [25], where analysis with a number of event shapes enables to constrain Yukawa coupling of light quarks. Studies of event shapes in Higgs decays includes fixed-order results at next-to-leading order (NLO) corresponding to $\mathcal{O}(\alpha_s^2)$ relative to the Born rate [26–30], resummed result of thrust at next-to-next-to-leading logarithmic accuracy (NNLL') for gluon channel [31], NNLL' matched to the NLO [32] and approximate N³LL' accuracy [33]. Angularity distributions are available at NNLL' for the quark channel, at NLL' for the gluon channel [34] and at NNLL in a groomed version for the gluon channel [35].

The angularity is a class of event shapes defined by a continuous weight parameter a that controls sensitivity

^{*} The work of DK, JZ, and YS is supported by the National Key Research and Development Program of China under Contracts No. 2020YFA0406301 and by the National Natural Science Foundation of China (NSFC) through Grant No. 12150610461. The work of JG was sponsored by the National Natural Science Foundation of China under the Grant No. 12275173 and No. 11835005. The work of TM is supported by the Science and Engineering Research Board (SERB) through the SRG (Start-up Research Grant) of File No. SRG/2023/001093.

1) E-mail: dkang@fudan.edu.cn

to the rapidity parameter as

$$\tau_a = \frac{1}{m_H} \sum_i |\mathbf{p}_\perp^i| e^{-|\eta_i|(1-a)}, \quad (1)$$

where m_H is the Higgs mass, the sum goes over all the final particle i having transverse momentum \mathbf{p}_\perp^i , and rapidity η_i is measured with respect to thrust axis, which is an axis minimizes the value of thrust $\tau_{a=0}$. For the change in a , the angularity τ_a is sensitive to a collinear particle having large rapidity $|\eta| \gg 1$ and less sensitive to a soft particle having smaller rapidity $|\eta| \sim \mathcal{O}(1)$. In other words, by regulating the value of a one can control relative contribution between the collinear and soft particles or modes. With its continuous parameter a , the angularity enables to interpolate parameter region between thrust ($a = 0$) and jet broadening ($a = 1$) and further extrapolate beyond this region. The infrared-safe region of angularity parameter a is $-\infty < a < 2$, where perturbation theory is valid. For the region $a \geq 2$, the angularity is sensitive to collinear splitting and becomes infrared-unsafe. In the framework of soft-collinear effective theory (SCET) [36–40], the factorization of angularity distribution in small τ_a region and resummation of Sudakov logarithms of τ_a are established and studied in thrust-like region $a < 1$ in e^+e^- [41–43] and in DIS [44], and the broadening-like region $a \sim 1$ in e^+e^- [45–47]. There are also studies of variants with recoil-free axis [48], with vector transverse momentum [49], and with joint two angularities [50]. In this work, we focus on improved prediction of the region $a < 1$.

The gluon channel starting at α_s^2 is known to suffer from large perturbative uncertainties compared to the quark channel. Angularity distribution for the gluon channel is only available at NLL', which is one-order lower than that of quark channel [34]. Improving the gluon channel, resummed up to NNLL' accuracy and matched up to next-to-leading order (NLO) accuracy, is the primary focus of this work. The most crucial part of it is to determine a remaining term, 2-loop constant of gluon-jet function in factorization and to compute the fixed-order distribution at NLO for angularity in Higgs hadronic decay.

Our paper is organized as follows. We first review factorization formula for angularity distribution in Sec. 2, which is used for resummation of logarithmic terms. In Sec. 3.1 we review the determination strategy of jet-function constant that makes use of a fit to fixed-order distribution, in Sec. 3.2 we discuss the one-loop constant to illustrate a fit form with fractional power, then in Sec. 3.3 we determine two-loop constant in the quark- and gluon-jet function using Tikhonov regularization to

handle ill-posed fit. In Sec. 4 we present our prediction of angularity distribution resummed at NNLL' accuracy and matched to NLO fixed-order distribution, and discuss leading and subleading nonperturbative corrections. Finally, we conclude in Sec. 5.

2 Factorization and resummation

At the small angularity limit, the final state hadrons can be treated as nearly back-to-back jets in the rest frame of the Higgs boson. Similar to the $e^+e^- \rightarrow q\bar{q}$, in the framework of soft-collinear-effective theory (SCET) [36, 37, 39, 51, 52], the factorization formula for the Higgs boson decay is given by [26, 41, 42]

$$\begin{aligned} \frac{d\Gamma^i}{d\tau_a} &= \Gamma_B^i(\mu) |C_t^i(m_t, \mu)|^2 |C_S^i(m_H, \mu)|^2 \int d\tau_a^{J1} d\tau_a^{J2} d\tau_a^S \\ &\times \delta\left(\tau_a - \tau_a^{J1} - \tau_a^{J2} - \tau_a^S\right) J^i(\tau_a^{J1}, \mu) J^i(\tau_a^{J2}, \mu) S^i(\tau_a^S, \mu), \end{aligned} \quad (2)$$

where $i = q, g$ represent the quark and gluon channel, respectively. The Born decay rates are $\Gamma_B^g(\mu) = \frac{m_H^3 \alpha_s^2(\mu)}{72\pi^3 v^2}$ and $\Gamma_B^q(\mu) = \frac{m_H C_A y_q^2(\mu)}{16\pi}$. The Wilson coefficient $C_t^g(m_t, \mu)$ corresponds to the top-quark loop coupled to two gluons [53–58], while for quark $C_t^q(m_t, \mu) = 1$. $C_S^i(m_H, \mu)$ represents the hard coefficient that can be found by integrating out the hard fluctuations near to the hard scale m_H . This hard coefficients are defined from the matching to SCET and can be obtained from $Hq\bar{q}$ and Hgg form factors that are available up to the 3-loop order [41, 59–61]. The angularity soft functions $S^i(\tau_a, \mu)$ describing soft emissions is available up to 2-loop order [43, 62, 63] for both quark and gluon, which are related by the Casimir scaling. The angularity jet functions $J^i(\tau_a, \mu)$ describe the collinear emission along the direction of initial quark or gluon. The quark-jet function is known up to 2-loop, and the gluon-jet function at the 1-loop [42, 43] is known a while ago while a remaining constant term in 2-loop gluon-jet function became available recently [64]. Here, one of the main tasks of this paper is to independently compute the 2-loop constant by using method described in Sec. 3.

In Eq. (2), the convergence in perturbation theory may break down due to the presence of Sudakov logarithms of τ_a . At small τ_a limit the logarithm shows singular behavior. A standard way to cure this behavior is through resummation of these large logs in momentum space [65, 66] or in Laplace space [67, 68]. Here we work in the Laplace space, where the transformation and factorization in Eq. (2) read as

$$\begin{aligned}\tilde{\Gamma}^i(\nu_a) &= \int_0^\infty d\tau_a e^{-\nu_a \tau_a} \frac{d\Gamma^i}{d\tau_a} \\ &= \Gamma_B^i(\mu) |C_t^i(m_t, \mu)|^2 |C_S^i(m_H, \mu)|^2 \tilde{J}^i(\nu_a, \mu) \tilde{J}^i(\nu_a, \mu) \tilde{S}^i(\nu_a, \mu),\end{aligned}\tag{3}$$

where ν_a is the conjugate variable, and \tilde{J}^i and \tilde{S}^i are the jet and soft functions in the Laplace space.

A generic form of $G = \{C_t, C_s, \tilde{J}, \tilde{S}\}$ in the fixed-order expansion in the strong coupling constant α_s is given in Eq. (23), that are composed of cusp $\Gamma(\alpha_s)$, non-cusp $\gamma(\alpha_s)$ anomalous dimensions, and constant terms. The large logs present in each function G are resummed by the renormalization group (RG) evolution starting from natural scales μ_G to the desired scale μ , where the scales μ_G are chosen as a physical momentum that minimizes the logs. Details of resummation are summarized in App. A and App. B.

At each order of α_s , $\log L$ terms behave like $\alpha_s^n L^k$, where $0 \leq k \leq 2n$. In logarithmic accuracy, the power counting of $\log L$ is $\alpha_s L \sim \mathcal{O}(1)$. Then, terms scaling like $\alpha_s^n L^{n+1} \sim \mathcal{O}(1/\alpha_s)$ are called leading log (LL), terms

like $\alpha_s^n L^n \sim \mathcal{O}(1)$ are next-to-leading log (NLL), and terms like $\alpha_s^n L^{n-k} \sim \mathcal{O}(\alpha_s^k)$ are N^kLL. At LL accuracy, the cusp anomalous dimension $\Gamma(\alpha_s)$ of each function and QCD beta function $\beta(\alpha_s)$ are needed, and at NLL accuracy, non-cusp anomalous dimensions $\gamma(\alpha_s)$ begins to contribute, and at NNLL accuracy, 1-loop constant terms are needed. At our target accuracy NNLL' 2-loop, constant terms should be added to NNLL accuracy. Table 1 summarizes the logarithmic accuracy and relevant n -order ingredients in α_s such as $\Gamma(\alpha_s), \beta(\alpha_s), \gamma(\alpha_s)$ and constant terms that are given in App. A and App. C.

Since our main focus is the gluon channel, computing the 2-loop constant term for the gluon-jet function and NNLL' resummation of the gluon channel, we set $i = g$ everywhere in Eqs. (2) and (3) and omit the superscript from now on.

	$\Gamma(\alpha_s)$	$\gamma(\alpha_s)$	$\beta(\alpha_s)$	constant in $\{C_t, C_s, J, S\}[\alpha_s]$
LL	α_s	1	α_s	1
NLL(')	α_s^2	α_s	α_s^2	$1(\alpha_s)$
NNLL(')	α_s^3	α_s^2	α_s^3	$\alpha_s(\alpha_s^2)$

Table 1. Resummation accuracy N^kLL and primed accuracy N^kLL'. Individual ingredients necessary at the corresponding accuracy: cusp and non-cusp anomalous dimensions, beta function, and hard, jet, and soft functions

3 Constant term of angularity jet function

In this section, we discuss a determination of the 2-loop constant term in the gluon-jet function necessary at NNLL' accuracy.

The constant is determined using NLO fixed-order result by following the strategy in [43, 60, 69]. In the determination, we introduce a fitting function, which improves numerical accuracy of the constant. The fitting function takes the asymptotic form for nonsingular part used in thrust [66] when $a \leq 0$ and contains additional terms with fractional powers associated with recoil corrections obtained in [45] when $a > 0$.

We first make a quick review of the strategy in Sec. 3.1. Then, we start with the one-loop constant by using LO result to illustrate and test recoil corrections in the fitting to nonsingular part in Sec. 3.2. In Sec. 3.3, we determine the two-loop constants of the quark- and gluon-jet functions by using NLO results in the quark

and gluon channels, respectively.

3.1 Review of determination strategy

The SCET factorization formula in Eq. (2) reproduces the singular terms of fixed-order QCD result when it is expanded and truncated at a fixed order in α_s . The singular part can be expressed as

$$\frac{1}{\Gamma_B} \frac{d\Gamma_s}{d\tau_a} = A\delta(\tau_a) + [B(\tau_a)]_+, \tag{4}$$

where the rate is normalized by the Born rate $\Gamma_B = \Gamma_B(m_H)$ at $\mu = m_H$, a constant term A contains contributions from constant terms of jet function as well as soft and hard functions, and the subscript $+$ on a function B implies the plus distribution in τ_a . The term A is also contained in the fixed-order QCD result, which can be expressed as sum of singular part in Eq. (4) and a nonsingular part $r(\tau_a)$ as

$$\frac{1}{\Gamma_B} \frac{d\Gamma}{d\tau_a} = A\delta(\tau_a) + [B(\tau_a)]_+ + r(\tau_a). \tag{5}$$

Because the same A appears in Eqs. (4) and (5), the constant of jet function can be determined from the fixed-order result. However, in practice the analytical results at NLO that can capture the delta function term Eq. (5) is not available for the angularity distribution.

We numerically compute the angularity distribution by using the codes used in predictions of thrust distribution [26], where matrix elements are generated by OPENLOOPS[72–74] in part and the phase space is integrated by Monte Carlo (MC) simulation with Vegas algorithm [75]. The numerical computation cannot capture term A due to the delta function $\tau_a = 0$ in Eq. (5), so we use total decay rate Γ_t , which is the integration of Eq. (5) and given in [71] for the quark channel and [55] for the gluon channel. The rate takes the following form

$$\frac{\Gamma_t}{\Gamma_B} = \int_0^1 d\tau'_a \frac{1}{\Gamma_B} \frac{d\Gamma}{d\tau'_a} = A + r_c, \quad (6)$$

where the plus distribution B in Eq. (5) vanished up on integration and r_c is a reminder function $r_c(\tau_a, 1)$ at $\tau_a = 0$, that is defined by accumulated nonsingular part $r(\tau_a)$ from τ_a to 1 as

$$r_c(\tau_a, 1) = \int_{\tau_a}^1 d\tau'_a r(\tau'_a) = \int_{\tau_a}^1 d\tau'_a \frac{1}{\Gamma_B} \left(\frac{d\Gamma}{d\tau'_a} - \frac{d\Gamma_s}{d\tau'_a} \right). \quad (7)$$

In the last equality, $r(\tau_a)$ is estimated by taking a difference between Eqs. (4) and (5).

Note that in numerical approach, we cannot compute Eq. (7) at $\tau_a = 0$. The remainder function is computed down to small $\tau_a \ll 1$ regions instead, and an approximate value of r_c is obtained by taking a fit using an

asymptotic form in the region and extrapolating the fit to $\tau_a = 0$. Then, the value of A can be obtained by subtracting the approximate value from Eq. (6). The fit method improves the accuracy of A determination. For example, in thrust limit, the error of A at NLO in gluon channel reduces from 2.6 % to 0.7 % using the fit with data above $\tau_a = 10^{-4}$ and this corresponds to a reduction from 20 % to 5 % in the constant term.

3.2 One-loop constant

In this subsection, we discuss the determination of one-loop constant by using LO QCD result in order to illustrate the fit to nonsingular part and to test the effect of recoil corrections.

We obtain the LO angularity distribution from 10^{10} MC events and bin the distribution in logarithmic space. In Fig. 1, the MC distribution in the gluon channel is compared with singular distribution at three values of angularity parameter $a = -1, 0$, and 0.5 . In the limit of $\tau_a \rightarrow 0$, as expected, the MC agrees well with the singular part, while in relatively large τ_a region they show significant differences due to large nonsingular part.

Then, we obtain nonsingular results $r(\tau_a)$, as shown in Fig. 2, by taking the difference between MC and singular results. In $a \leq 0$, the nonsingular $r(\tau_a)$ follows an asymptotic form as

$$\sum_{k=0}^1 \alpha_k \ln^k \tau_a. \quad (8)$$

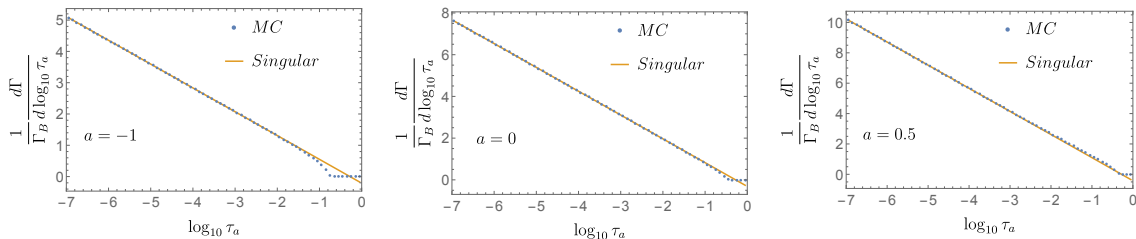


Fig. 1. LO MC distribution (dots) and singular distribution (solid line) in gluon channel.

One can fit with above form to the nonsingular part to improve accuracy in the small τ_a region when the data suffers from large uncertainties.

On the other hand, for $a > 0$, the nonsingular part has subleading singular terms that are more significant contributions than those in Eq. (8) and become increasingly large with increasing a . According to SCET power counting of angularity, collinear and soft momenta re-

spect following scaling:

$$p_c^\mu \sim Q(\lambda^2, 1, \lambda) \quad \text{and} \quad p_s^\mu \sim Q\lambda^{2-a}, \quad (9)$$

where λ is a small parameter in SCET and defined by the observable $\lambda^{2-a} \sim \tau_a$. The collinear momentum p_c^μ along a unit vector \hat{n} is expressed in the light-cone coordinates and the three components are $n \cdot p_c$, $\bar{n} \cdot p_c$, and p_c^\perp where $n = (1, \hat{n})$ and $\bar{n} = (1, -\hat{n})$. For angularity $a \lesssim 0$, the thrust axis is insensitive to transverse recoil by soft

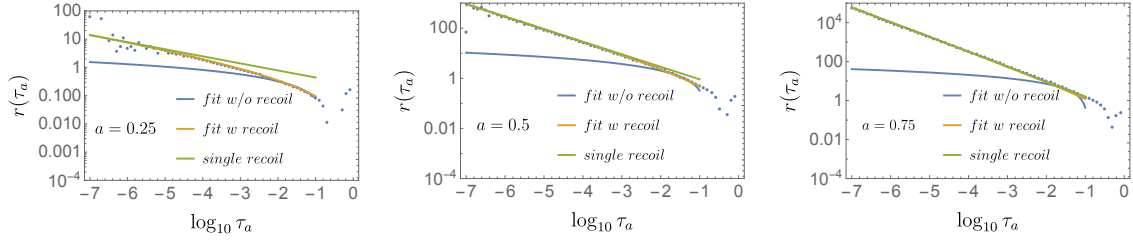


Fig. 2. LO nonsingular part (dots) and fit results with and without recoil corrections (blue and orange, respectively) and fit only with recoil corrections

radiation, i.e., $p_c^\perp \gg p_s^\perp$, but for $a \rightarrow 1$, the recoil effect is significant, i.e., $p_c^\perp \sim p_s^\perp$. The recoil corrections obtained from one-loop soft function in [45] are given by

$$-\frac{\alpha_s C_i}{\pi} \frac{4}{2-a} \sum_{n=1}^{\lceil 1/(1-a) \rceil - 1} \frac{c_n}{\tau_a^{1-n(1-a)}}, \quad (0 < a < 1) \quad (10)$$

where the color factor $C_i = C_F$ and C_A for quark and gluon channels, respectively and $\lceil x \rceil$ is the *ceiling function*. The series sum turns into a single term $\frac{c_1}{\tau_a^a}$ for $a \in (0, 1/2]$, two terms $\frac{c_1}{\tau_a^a} + \frac{c_2}{\tau_a^{2a-1}}$ for $a \in (1/2, 2/3]$, three terms $\frac{c_1}{\tau_a^a} + \frac{c_2}{\tau_a^{2a-1}} + \frac{c_3}{\tau_a^{3a-2}}$ for $a \in (2/3, 3/4]$, and so on. The recoil corrections are characterized by the fractional power, which is still suppressed compared to the singular terms $\ln^n \tau_a / \tau_a$, but they are greater than typical power corrections $\ln^n \tau_a$ in Eq. (8). The coefficients c_n for $n = 1, 2, 3$ are given by

$$c_1 = -1, \quad c_2 = \frac{1}{2}(3-2a), \quad c_3 = -\frac{1}{6}(20-27a+9a^2). \quad (11)$$

In our fit, the coefficients are set to free parameters that are determined by the fit to data. The effect of recoil corrections is shown in Fig. 2, where three fit results using a form in Eq. (8) without any recoil corrections (blue), a form with both Eq. (8) and Eq. (10) (orange), and a form with just recoil terms in Eq. (10) without Eq. (8) (green). We find that the fitting results in orange and in green agree with Eq. (11).

At $a = 0.25$, the fit with both terms in Eqs. (8) and (10) works, while at $a = 0.5$ and 0.75 , the fit with just recoil terms in Eq. (10) can mostly describe the data. As a increases, the recoil corrections become larger and dominate over typical power corrections in Eq. (8), and the fit without the recoil cannot describe the behavior of nonsingular data.

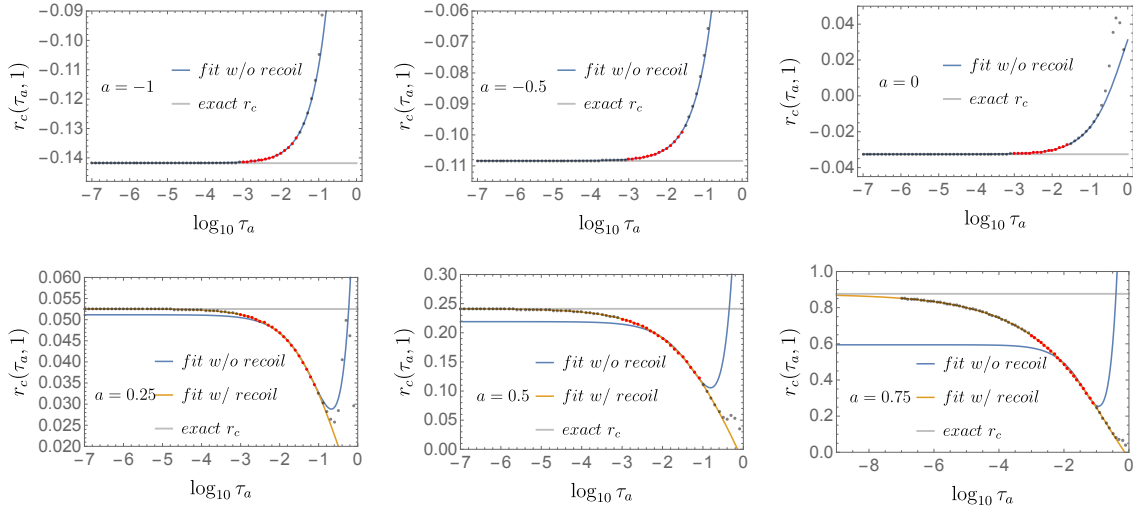


Fig. 3. Remainder function (dots) at LO in gluon channel, fit result with and without recoil corrections (blue and orange respectively) to data in fit regions (red).

Fig. 3 shows the remainder function $r_c(\tau_a, 1)$ (dots) obtained by integrating $r(\tau_a)$ in Fig. 2, fit curves similar to Fig. 2, and exact value of r_c (horizontal gray line) obtained from exact singular part and LO total rate. In selection of fit regions (red), plateau regions are excluded in order to test the prediction of the fit result.

The fits with recoil corrections extrapolate well to the exact values of r_c in $a > 0$, while fits without recoil corrections extrapolate well to the exact value in $a \leq 0$

and begin to deviate from the value for $a > 0$. The fact that data for $r_c(\tau_a, 1)$ shows plateau region, which is well aligned with the exact value of r_c , does not motivate such fit and extrapolation since fine-tuning errors in the difference between LO fixed-order and singular part is not significant compared to those at NLO. We again emphasize that the purpose of this subsection is to illustrate the significance of including recoil corrections shown in the fits and motivate NLO fit with those terms.

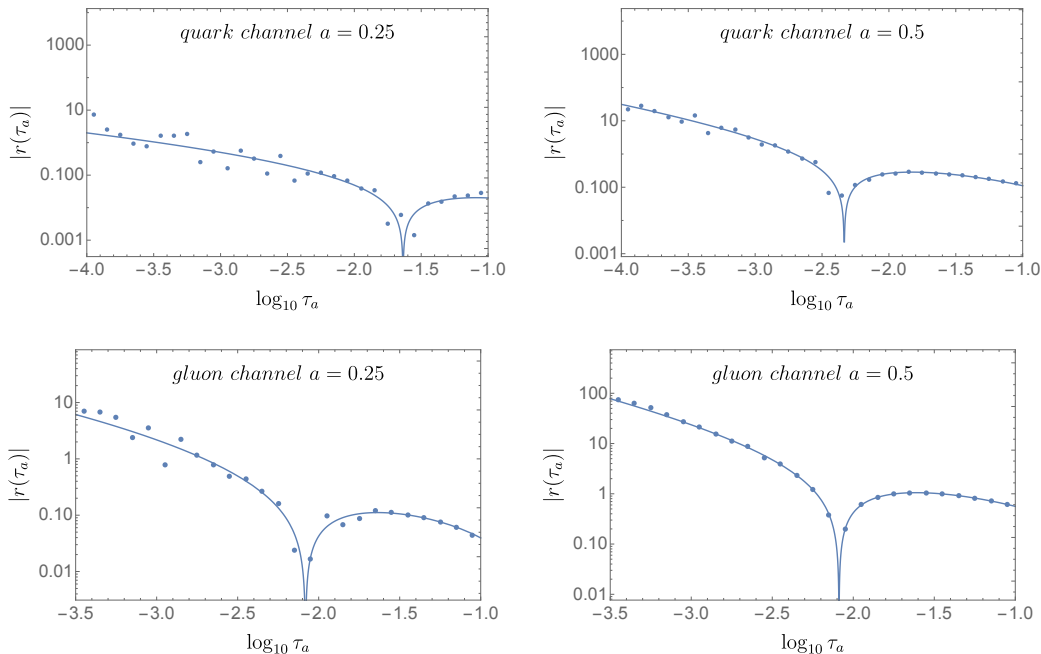


Fig. 4. NLO nonsingular parts (dots) at $a = 0.25$ and 0.5 for quark (upper) and gluon (lower) channels and fit curves (blue) including recoil corrections

3.3 Two-loop constants

Following the same strategy, we determine the two-loop constant of jet function by using NLO total rate [55], NLO fixed-order obtained from MC simulations, and two-loop singular part obtained from Eq. (2).

We also perform a fit to the nonsingular part by including recoil-correction terms for $a > 0$. However, their scaling behavior at NLO is currently unknown. We make a conjecture for regarding the scaling behavior, test this conjecture in the quark channel, and then apply it to the gluon channel. Our conjecture is that dominant scaling behavior can be inferred from crossing terms between the one-loop jet function and recoil corrections from the one-loop soft function. In this conjecture, we assume that recoil-corrections from the two-loop soft function and one- and two-loop jet functions will not produce more

singular terms. The convolution of singular terms $\ln^k \tau_a$ from the jet function and recoil corrections of a form in Eq. (10) gives

$$\sum_{n=1}^{\lceil 1/(1-a) \rceil - 1} \sum_{k=0}^2 \alpha_{n,k} \frac{\ln^k \tau_a}{\tau_a^{1-n(1-a)}}, \quad (12)$$

where $\alpha_{n,k}$ are fit parameters. For the region $0 < a \leq 1/2$, $n = 1$ and Eq. (12) reduces to

$$\sum_{k=0}^2 \alpha_{1,k} \frac{\ln^k \tau_a}{\tau_a^a}. \quad (0 < a \leq 1/2). \quad (13)$$

We also need to include typical integer-power corrections of the form

$$\sum_{k=0}^3 \alpha_k \ln^k \tau_a, \quad (14)$$

where α_k are fit parameters. These terms are leading contributions for $a \leq 0$ since there are no recoil corrections in Eq. (12). The form in Eq. (14) turns into $r_c + \tau_a \sum_{k=0}^3 \tilde{\alpha}_k \ln^k \tau_a$ in the remainder function $r_c(\tau_a, 1)$, and the value of r_c is determined from the fitting to $r_c(\tau_a, 1)$ data obtained from Eq. (7).

A subtlety of the fit with recoil corrections in $a > 0$ is that eight or more fit parameters make the fit ill-posed, and an ordinary chi-square fit cannot constrain those parameters properly. We adopt Tikhonov regularization [76], in which a regularization term $\lambda |\Gamma \mathbf{x}|^2$ is added to the chi-square and tames the ill-posed fit, where λ is a regularization parameter and Γ is a Tikhonov matrix. More details about the regularization and our choice of λ and Γ are discussed in App. D.

Fig. 4 shows the nonsingular part of angularity distribution in the quark and gluon channel at $a = 0.25$ and 0.5 and, along with fitting results using terms in both Eqs. (12) and (14). The fit curves well describe data. We also looked into the small τ_a region beyond the range in the figure and checked the relative importance of the leading-log term in Eq. (12). At $a = 0.25$, the fit result with the leading-log is qualitatively similar to that with all three terms in Eq. (12). However, at $a = 0.5$, just leading-log cannot explain the data and including subleading-log terms in the fit form makes significant improvement. Therefore, we include all three terms from Eq. (12) in our fit.

Once r_c is determined from the fit, one can obtain the two-loop constant c_j^2 from the following relation

$$r_c = -2 \left(\frac{\alpha_s}{4\pi} \right)^2 c_j^2 + \Delta_a, \quad (15)$$

where $\Delta_a = \Gamma_t/\Gamma_B - \left[A - 2 \left(\frac{\alpha_s}{4\pi} \right)^2 c_j^2 \right]$ is obtained by rewriting Eq. (6) and the term in square bracket is simply the sum of all contributions except for missing c_j^2 hence, is known from the singular part. We determine the constants at seven values of $a = -1 + n/4$, where $n = \{0, \dots, 6\}$, for which numerical values of Δ_a for quark and gluon channels are

$$\begin{aligned} \Delta_a^{\text{quark}} &= \{-0.0301, -0.0273, -0.0243, -0.0207, \\ &\quad -0.0157, -0.0082, 0.0036\}, \\ \Delta_a^{\text{gluon}} &= \{-0.1598, -0.1474, -0.1319, -0.1106, \\ &\quad -0.0787, -0.0258, 0.0695\}, \end{aligned} \quad (16)$$

where we set $\alpha_s = 0.1127$.

3.3.1 quark channel

According to the procedure described in previous sections, we numerically obtain the remainder function $r_c(\tau_a, 1)$ in the quark channel at seven values of angularity parameters from 10^{11} MC events computed on Intel Xeon Platinum 9242 CPU for about 3k CPU hrs with an

IR cutoff $\alpha_{\text{cut}} = 10^{-11}$ on a dimensionless variable $y_{i,j,k}$ in the dipole subtraction [77–79].

The remainder function in Fig. 5 tends to have larger uncertainties in the small τ_a region around 10^{-4} and below, due to fine-tuning with large cancellations between fixed-order and singular parts. In the plots for $a \leq 0$, one can read plateau regions approaching existing results [43] (horizontal gray line) and determine r_c , hence two-loop constant c_j^2 using Eq. (15). The value of r_c is determined by extrapolating the fit curve (blue) to $\tau_a = 0$ with a fit form obtained by integrating Eq. (14). In selection of the fit region (red dots with error bar), we eliminated the plateau region to test the asymptotic forms.

On the other hand, for $a > 0$, a plateau is hardly observed from data, and two fit results with and without recoil corrections (orange and blue) are shown in the figure, respectively. Plateau region would appear in smaller τ_a region as a increases because the recoil corrections like $\tau_a^{n(1-a)}$ make convergence of the remainder functions further slow. It is not accessible from MC results computed with double precision of machine variables. As indicated in Fig. 4, the fit with recoil corrections at $a = 0.5$ clearly extrapolates to the value of r_c close to existing value [64, 80] (horizontal gray line). Our values of c_j^2 are given in Table 2 and show reasonable agreement with existing results in [43, 64, 80]. We note that our fit region does not include the plateau region, and our results in Table 2 tend to have larger uncertainties than those that could have been obtained from the best fit including the plateau region, because our purpose in the quark channel is to verify fitting with the asymptotic form.

In the fit region (red dots with error bar), we take a set of fit regions $\{\tau_a^{\text{low}}, \tau_a^{\text{high}}\}$ and obtain a set of r_c values and statistical uncertainties from fitting to the regions. For the systematic uncertainty, which mainly comes from the IR cutoff and higher-power corrections, we take the maximum deviation of r_c from its averaged value in the set. We obtain our central value from the averaged r_c , and our uncertainty from the sum of the systematic and averaged-statistical uncertainties in quadrature. Specifically, the set $\{\tau_a^{\text{low}}, \tau_a^{\text{high}}\}$ is obtained from all possible combinations for pair from 9 succeeding points for $\log_{10} \tau_a^{\text{low}}$ domain, separated by a step size of 0.1, and similarly 5 succeeding points for $\log_{10} \tau_a^{\text{high}}$ domain. Our selection criteria for τ_a^{high} domain is that it should be robust against higher-power corrections and we select $\{-1.6 + 0.4(1+a), -1.2 + 0.4(1+a)\}$. The criteria for τ_a^{low} domain is that it should be insensitive to IR cutoff. We scan all available domains of 9 succeeding points and select the domain giving least that gives the least standard deviation for r_c . We also explore the effect of the cutoff α_{cut} by comparing our standard value $\alpha_{\text{cut}} = 10^{-11}$ with larger value 10^{-8} in App. E

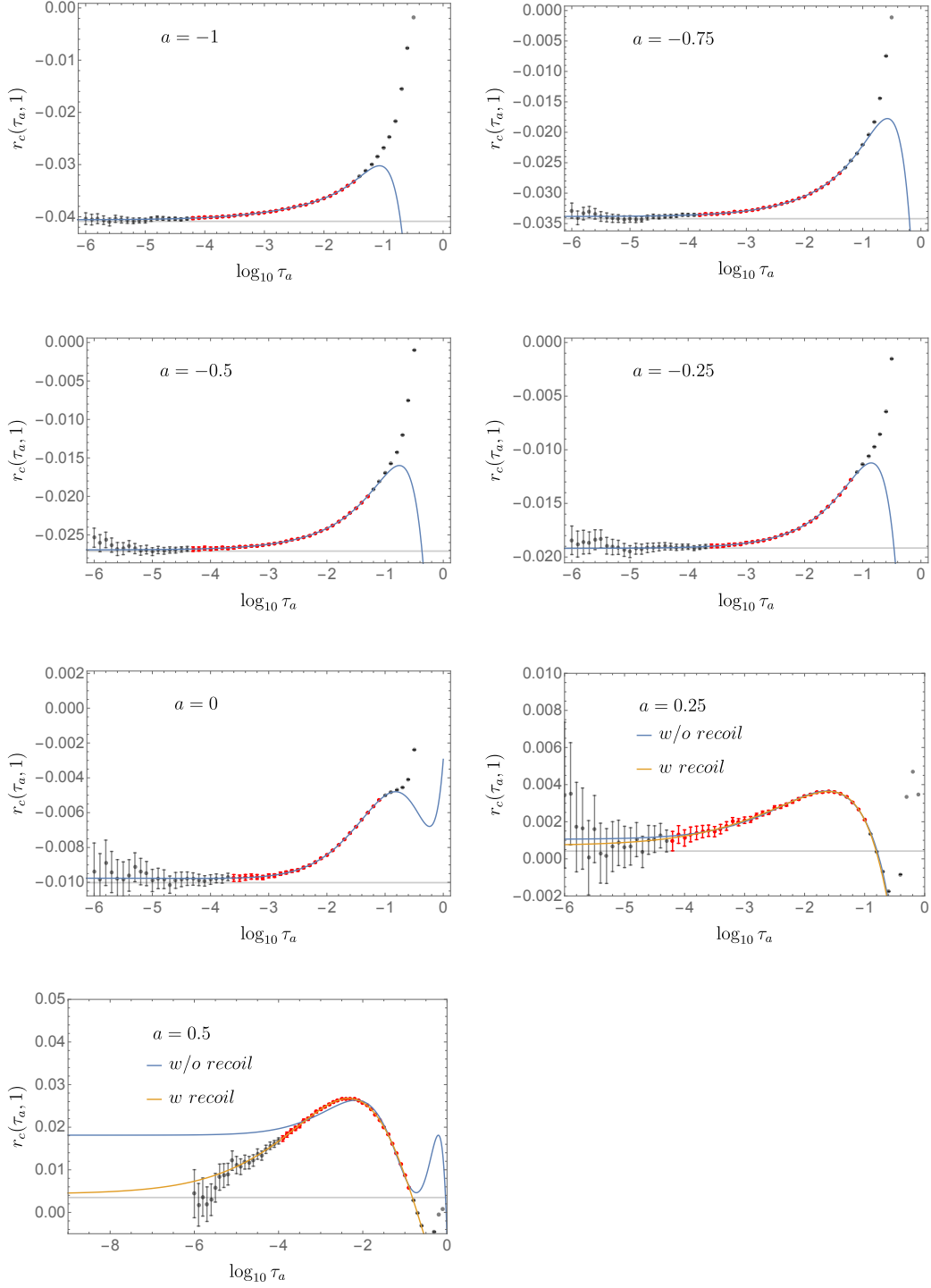


Fig. 5. NLO remainder function $r_c(\tau_a, 1)$ (gray and red dots with error bar) in the quark channel, and fit results without recoil corrections (blue) and with the corrections (orange) to the selected region of data (red dots with error bar) compared with existing values of r_c (horizontal gray line)

Table 2. Two-loop constant c_j^2 of quark-jet function for angularity

$c_j^2 \setminus a$	-1	-0.75	-0.5	-0.25	0
this work	65.43 ± 0.91	40.41 ± 1.02	16.52 ± 0.36	-9.10 ± 1.16	-36.84 ± 0.72
Ref. [43]	$66_{-3.5}^{-5.2}$	$42.3_{-3.3}^{+5.1}$	$17.3_{-2.5}^{+3.2}$	$-9.34_{-2.48}^{+2.76}$	$-36.3_{-2.4}^{+2.7}$
Ref. [64]*	67.8	43.1	18.2	-8.7	-34.9
	0.25	0.5			
	-55.36 ± 0.69	-3.18 ± 2.13			
	$-57.6_{-3.2}^{+3.8}$	$-79.8_{-24.9}^{+39.7}$			
	-53.6	-0.22			

* The values are read from plots in the thesis and would have errors of a few percent.

3.3.2 gluon channel

Now we determine the two-loop constant of the angularity gluon-jet function and compare our results to values given in [64]. The procedure is essentially the same as that described in Sec. 3.3.1, and we only describe the difference from that section.

We use the same number of 10^{11} MC events with larger cutoff $\alpha_{\text{cut}} = 10^{-8}$ in the gluon channel. Fig. 6 shows NLO remainder function $r_c(\tau_a, 1)$ (gray and red dots with error bar) obtained from MC events, compared with fit results (blue) for the selected region of data (red dots) and r_c values in [64] (horizontal gray line). The fits for $a \leq 0$ were performed without the recoil corrections

while for $a > 0$ with the recoil corrections. Unlike the quark channel, we do not observe any plateau regions at any value of a hence, fitting with asymptotic form in Eqs. (12) and (14) is essential in the gluon channel.

Due to more severe cutoff effect, the fit regions are narrowed. The domains of $\log_{10} \tau_a^{\text{low}}$ reduces to 7 succeeding points for non-positive a and $\log_{10} \tau_a^{\text{high}}$ to 5 points for positive a .

The cutoff effect on the value of c_j^2 in the gluon channel is shown in App. E. Table 3 shows our two-loop constant c_j^2 converted from r_c values by using Eq. (15), and our values show reasonable agreement with those values reported in [64].

 Table 3. two-loop constant c_j^2 of gluon-jet function for angularity

$c_j^2 \setminus a$	-1	-0.75	-0.5	-0.25	0
this work	44.19 ± 1.70	2.10 ± 2.75	-36.43 ± 1.65	-62.08 ± 2.49	-54.55 ± 2.60
Ref. [64]*	37.18	-4.59	-40.27	-56.95	-55.73
	0.25	0.5			
this work	75.09 ± 10.99	814.48 ± 28.71			
Ref. [64]*	69.21	776.61			

* The values are read from plots in the thesis and would have errors of a few percent.

4 Angularity distributions at NNLL' matched to NLO

In this section, we present the angularity distribution at NNLL' matched to fixed-order NLO results, which is $\mathcal{O}(\alpha_s^2)$ correction relative to the Born rate $\Gamma_B(\mu)$. The distribution is composed of two parts

$$\frac{1}{\Gamma_B} \frac{d\Gamma}{d\tau_a} = \frac{1}{\Gamma_B} \frac{d\Gamma^{\text{res}}}{d\tau_a} + r(\tau_a, \mu_{\text{ns}}), \quad (17)$$

where $\frac{d\Gamma^{\text{res}}}{d\tau_a}$ is the resummed-singular part, and $r(\tau_a, \mu_{\text{ns}})$ is the nonsingular part at a scale μ_{ns} , including all subleading-power corrections of τ_a at NLO. As described in Sec. 2, we perform the log resummation by RG-evolving the functions in factorization equation Eq. (3). We give a final expression in Eq. (54), and the detailed procedure is summarized in App. A and App. B. The nonsingular part makes our full distribution in Eq. (17) matched to fixed-order result as defined in Eq. (5). Including this is important because the unphysical behavior of singular terms in the large τ_a region can be

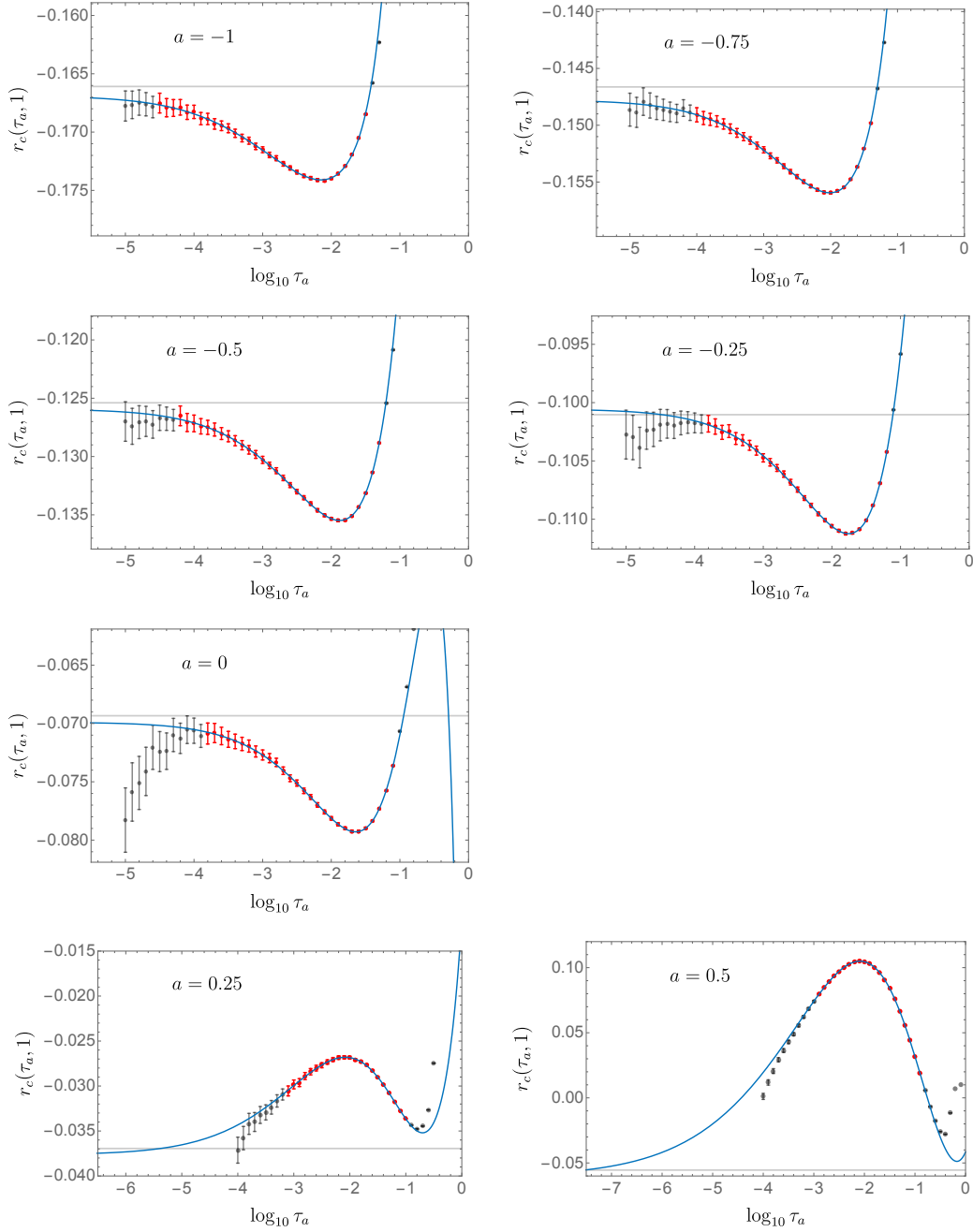


Fig. 6. NLO remainder function $r_c(\tau_a, 1)$ (gray and red dots with error bar) in the gluon channel, and fit results (blue) from the selected region (red dots with error bar) compared with existing values of r_c (horizontal gray line)

corrected by adding the nonsingular part. Note that in Eq. (17), $\Gamma_B = \Gamma_B(m_H)$ is the Born decay rate at the scale of Higgs mass hence, both the singular and nonsingular parts contain a prefactor $\Gamma_B(\mu)/\Gamma_B(m_H) = \alpha_s(\mu)^2/\alpha_s(m_H)^2$.

We also compute a cumulative distribution by integrating Eq. (17) from 0 to τ_a as

$$\begin{aligned} \frac{\Gamma_c(\tau_a)}{\Gamma_B} &= \int_0^{\tau_a} d\tau'_a \left[\frac{1}{\Gamma_B} \frac{d\Gamma^{\text{res}}}{d\tau'_a} + r(\tau'_a) \right] \\ &= \frac{\tau_a}{\Omega \Gamma_B} \frac{d\Gamma^{\text{res}}}{d\tau_a} + r_c(0, \tau_a), \end{aligned} \quad (18)$$

where $\Omega = \eta_S + 2\eta_J$ is the sum of integrated anomalous dimensions of the jet and soft functions, which are defined in Eqs. (40) and (41). When the resummation is turned off, Ω reduces to zero and cancels against the same factor in $d\Gamma^{\text{res}}/d\tau_a$ so that $\Gamma_c(\tau_a)$ remains finite.

4.1 Matching

The nonsingular part in Eq. (17) can be expressed in a scale independent form satisfying $dr(\tau_a, \mu)/d\mu = 0$ as

$$\begin{aligned} r(\tau_a, \mu_{\text{ns}}) &= \frac{\alpha_s(\mu_{\text{ns}})^2}{\alpha_s(m_H)^2} \left\{ \frac{\alpha_s(\mu_{\text{ns}})}{4\pi} r^1(\tau_a) \right. \\ &\quad \left. + \left(\frac{\alpha_s(\mu_{\text{ns}})}{4\pi} \right)^2 \left[r^2(\tau_a) + 3\beta_0 r^1(\tau_a) \ln \frac{\mu_{\text{ns}}^2}{m_H^2} \right] \right\}, \end{aligned} \quad (19)$$

where $r^1(\tau_a)$ and $r^2(\tau_a)$ are LO and NLO coefficients, respectively and only depend on τ_a . The scale dependency on μ_{ns} is made explicit with the logarithmic term proportional $3\beta_0 r^1$, which is cancelled by the same term generated by scale variation of lower-order term proportional to $r^1(\tau_a)$. In comparison to nonsingular part in e^+e^- angularity [43], the log term differs from that in [43] by a factor of 3 due to an additional prefactor $\alpha_s(\mu_{\text{ns}})^2$ from the Born rate $\Gamma_B^g(\mu)$, which is absent in e^+e^- angularity.

An analytic expression of the nonsingular part is unknown except for the thrust limit $a = 0$, and it is determined numerically from MC events obtained in Sec. 3.3. We interpolate the remainder function obtained from MC events instead of interpolating the nonsingular part because the binned-nonsingular part inherits uncertainties by an amount of bin size in x-axis associated while with its integration, remainder function, does not at the end of each bin. Then, we obtain the nonsingular part by taking the numerical differentiation of the interpolated remainder function.

In order to maintain good precision of the interpolation in both small and large τ_a regions, the spectrum of $r^n(\tau_a)$ is divided into two regions, below and above a point $\tau_a = 0.1$. Below the point, MC data is binned in log space from a lower bound $\log_{10} \tau_a^{\text{low}}$ to the point with a step size of 0.1, where the lower bound is -7 at LO and -4 or, -5 at NLO. Above the point, the MC data is binned in linear space τ_a up to 1 with a step size of 0.01. At NLO, MC data in small τ_a regions tends to be significantly biased by the cutoff effect as shown in Fig. 11, and the fit function is instead to describe points below $\tau_a = 0.1$. Then, interpolation functions $r_{\log_{10}}^n(\tau_a)$ and $r_{\text{lin}}^n(\tau_a)$ in two regions are joined smoothly following the method in [43]:

$$\begin{aligned} r^n(\tau_a) &= [1 - f(\tau_a, 0.1, 0.01)] r_{\log_{10}}^n(\tau_a) \\ &\quad + f(\tau_a, 0.1, 0.01) r_{\text{lin}}^n(\tau_a), \end{aligned} \quad (20)$$

where $f(z, z_0, \epsilon) = 1/(1 + e^{-(z-z_0)/\epsilon})$ is a transition function.

Nonsingular distributions with error bars at LO (first row) and at NLO (second row) are shown in Fig. 7, and red curves are the interpolations joined using Eq. (20). Note that the nonsingular is not a physical quantity and can be negative, while full distribution in Eq. (17) is physical and positive definite.

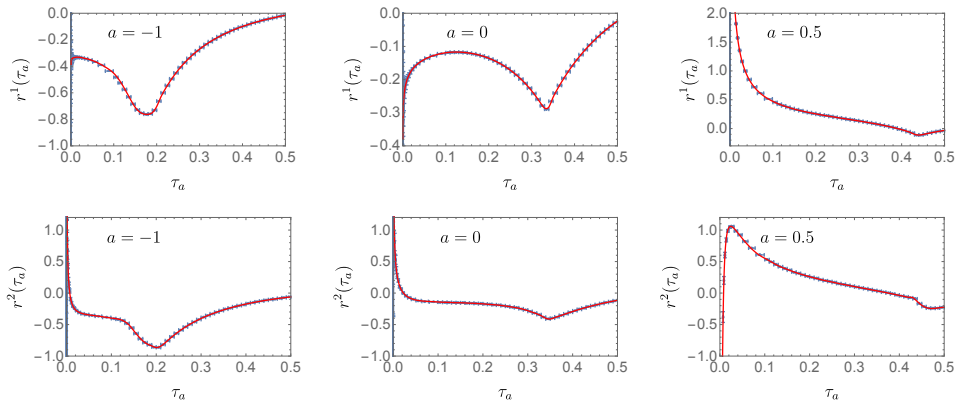


Fig. 7. LO (upper) and NLO (lower) coefficients of nonsingular part $r(\tau_a, \mu_{\text{ns}})$ at $a = -1, 0, 0.5$.

4.2 Numerical results

For the numerical calculation of distribution, one needs to make proper choice for the scales: hard scales μ_{C_t} , μ_{C_S} , soft scale μ_S and jet scale μ_J . In the choice one needs to consider the τ_a distribution divided by three regions: the peak region ($\tau_a \sim 2\Lambda_{QCD}/m_H \ll 1$), the tail region ($2\Lambda_{QCD}/m_H \ll \tau_a \ll 1$) and the far-tail region ($\tau_a \sim 1$). The tail region is the region where τ_a remains small and resummation is effective. In the region, the natural choice is the canonical scales $\mu_{C_t, C_S} = m_H$, $\mu_J = m_H \tau_a^{1/(2-a)}$, $\mu_S = m_H \tau_a$ that minimize the logarithms in each function. In far-tail region, $\mu_i \sim \mathcal{O}(m_H)$ and we can set all scales to be hard scale $\mu_i = m_H$, which is a conventional choice in fixed-order perturbation the-

ory. The peak region is dominated by nonperturbative (NP) effect and our perturbative approach is invalid. Before approaching the peak region, we need to stop scales running into Λ_{QCD} and make them frozen in perturbative region well above Λ_{QCD} . One can design *Profile function* $\mu_i(\tau_a)$ that is a smooth function of τ_a satisfying above criteria [65, 66, 81]. Here, we adopt the profile functions and scale variations to estimate perturbative uncertainty designed for the e^+e^- angularity in [43] and we modify a parameter $t_2(a)$ to be $0.43 \times 0.674^{1-1.913a}$, which is the value of τ_a where singular and nonsingular parts of the gluon channel are the same in size and beyond the point all scales smoothly transit to the hard scale. We also take the choice of [43] for a scale μ_{ns} in nonsingular part.

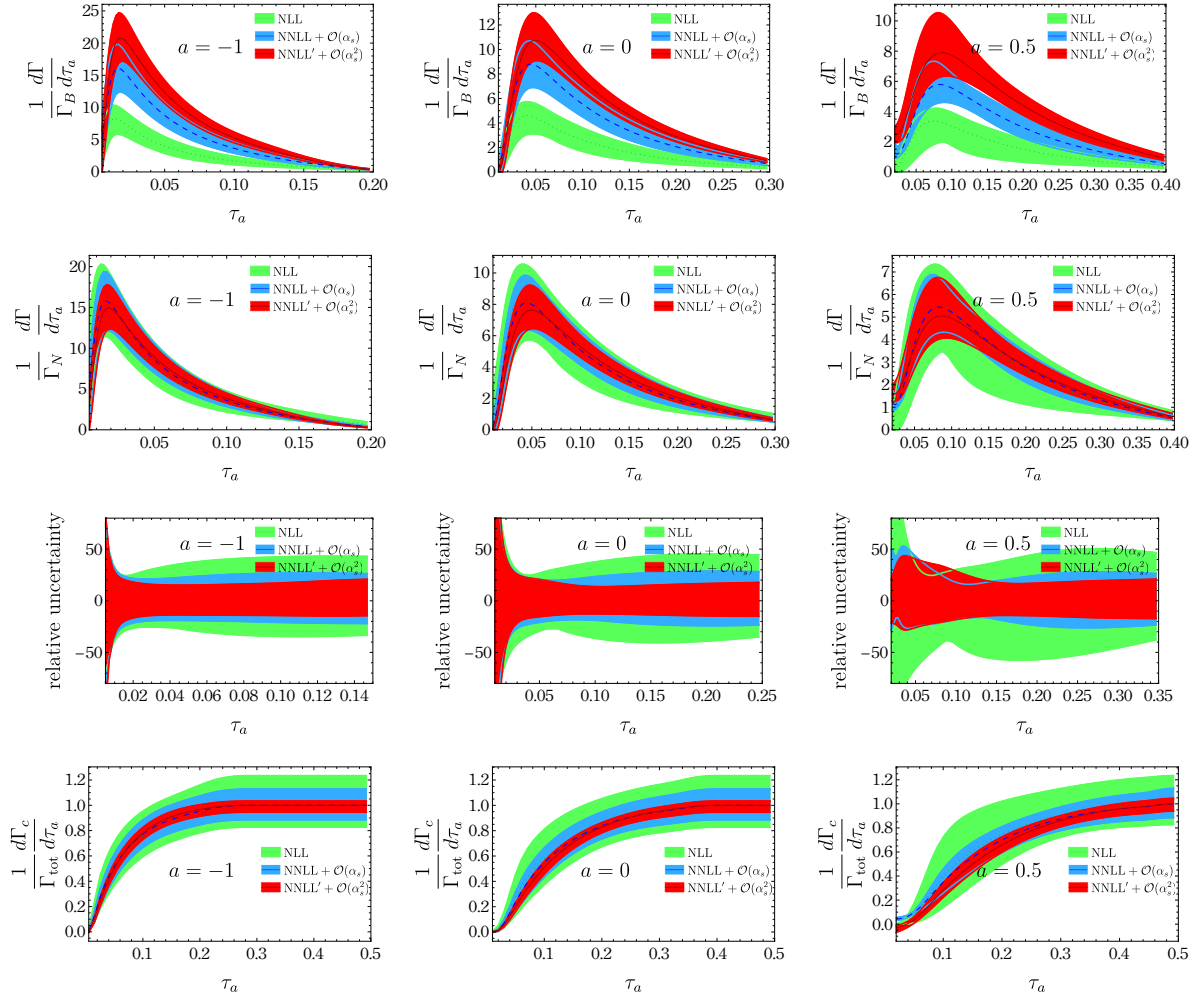


Fig. 8. First and second rows: Angularity distributions at three values of $a = -1, 0, 0.5$ for gluon channel in Higgs decay. The bands indicate perturbative uncertainties. The first row is normalized by the Born rate Γ_B and the second by area covered by resummed distribution Γ_N at corresponding order. Third row: Relative perturbative uncertainty in percentage. Bottom row: Cumulative distributions normalized by total rate.

Fig. 8 shows our resummed results at NNLL' + $\mathcal{O}(\alpha_s^2)$ accuracy (red) for angularity distribution (first and second rows), relative uncertainties (third row), and cumulative distributions (fourth row) at three values of $a = -1, 0, \text{ and } 0.5$ and results at lower accuracy: NLL (green) and NNLL + $\mathcal{O}(\alpha_s)$ (blue) for a comparison. Band at each accuracy represents perturbative uncertainty estimated by scale variations in the profile function. The distributions normalized by the Born rate in the first row hardly overlap between different accuracy, and the peak of distribution increases by 100 % from NLL to NNLL and 50 % from NNLL to NNLL' because of large perturbative corrections as in the total rate. The distributions normalized by their own area in the second row show reasonable overlapping within the uncertainties between different accuracy which indicates a perturbative convergence of the resummation. In the third row, the perturbative uncertainties with respect to central values reduce to about 20 % at NNLL', which is about half of NLL uncertainties, however the reduction rate with increasing accuracy is rather slow compared to the quark channel as many gluon initiated processes do. c_j^2 uncertainties in Table 3 propagate to the distribution and the values also show deviations from 2-loop results in Ref. [64], their effect in the distribution are as large as 0.8%, which is negligible compared to the perturbative uncertainties at this level of accuracy. In the fourth row, the cumulative distribution is normalized by the total rate at corresponding order in α_s . One can observe the cumulative distribution reduces to the total rate in the far-tail region. In the region resummation is turned off and resummed distribution in Eq. (17) reduces to the fixed-order result in Eq. (5).

One can observe a generic feature of the distribution that the shape becomes broad and the peak moves to right with increasing a because for a given jet scale $\mu_J = m_H \tau_a^{1/(2-a)}$, increasing a scales up the value of τ_a . But this is not true for the soft scale $\mu_S = m_H \tau_a$, where a does not change the scale of τ_a . Both of them affect the distribution and make its change as a function of a non-trivial. The peak of the distribution is essential feature of the resummation known as Sudakov exponent, which is $e^{-\frac{2\alpha_s C_A}{\pi} \ln^2 \tau_a}$ at LL accuracy, and cures the singular behavior $\ln \tau_a / \tau_a$ and the peak position of gluon channel is rather located at large τ_a compared to that in the quark channel due to the Casimir scaling.

Fig. 8 shows pure perturbative contribution without the NP effect like hadronization that can be included by introducing a NP model [65, 82, 83] or, power correction with a universal NP parameter $\Omega \sim \mathcal{O}(\Lambda_{\text{QCD}})$ [84], which can be further refined with a scheme subtracting renormalon ambiguities [69, 85]. The parameter Ω captures a leading NP correction and shifts the perturbative

distribution, hence the first moment of τ_a as

$$\langle \tau_a^{\text{had}} \rangle = \langle \tau_a^{\text{pert}} \rangle + \frac{2}{1-a} \frac{\Omega}{m_H} + \mathcal{O}(\Lambda_{\text{QCD}}^2/m_H^2), \quad (21)$$

where the superscript 'had' is for the hadron level that can be measured in experiment, or simulated in event generators, and 'pert' is for pure perturbative result at the parton level. Eq. (21) includes the quark and gluon channel $\Omega = f_q \Omega_q + f_g \Omega_g$, where $f_i = \Gamma_{tot}^i / (\Gamma_{tot}^q + \Gamma_{tot}^g) \approx 0.9$ and 0.1 for the quark and gluon fractions, respectively. For the quark channel $\Omega_q^{ee} \approx 0.35$ GeV from the e^+e^- thrust analysis [66] and assuming Casimir scaling estimates $\Omega_g \approx C_A/C_F \Omega_q$. We can determine Ω_g in Higgs factories by using the known value of Ω_q^{ee} .

Eq. (21) predicts a dependence $(1-a)^{-1}$ in Ω term that can be easily identified by comparing experiment and theory predictions in a space [86]. We can also test if the a dependence in Ω term is comparable with the hadronization model in event generators. Fig. 9 shows the difference $\langle \tau_a^{\text{had}} \rangle - \langle \tau_a^{\text{pert}} \rangle$ with a weight $(1-a)m_H$ obtained from Pythia simulations for the quark channel and gluon channel. The y values correspond to $2\Omega_q$ for the quark and $2\Omega_g$ for the gluon and would weakly depend on a via subleading term $\mathcal{O}(\Lambda_{\text{QCD}}^2/m_H^2)$ in Eq. (21). While the quark channel is consistent with the a dependence and $\Omega_q^{\text{pythia}} \approx 0.2$ GeV roughly agreeing with Ω_q^{ee} within a factor of two, the gluon channel shows rather stronger a dependence ranging $\Omega_g^{\text{pythia}} \approx 0.2 \sim 0.6$ GeV order of Λ_{QCD} . Their relative contributions are $f_q \Omega_q^{\text{pythia}} \approx 0.2$ and $f_g \Omega_g^{\text{pythia}} \approx 0.02 \sim 0.06$, where the gluon contributions are suppressed and the a dependence would become soft. Measurements in future Higgs factories can justify the value of Ω_g . If Pythia value is different from the measurement, it could come from another source such as large perturbative corrections at higher orders absent in Pythia that have been absorbed into hadronization parameters fitted to experimental data.

The subleading NP corrections of $\mathcal{O}(\Lambda_{\text{QCD}}^2/m_H^2)$ in Eq. (21) can be studied from higher-moment or cumulant analysis. In e^+e^- thrust [87], 2nd thrust cumulant, which is completely insensitive to Ω^q enabled to determine a subleading correction $\Omega_2^q(0)$, which is the sum of two contributions: one from leading thrust factorization and the other from a power correction $\Omega_{1,1}^q(0) \sim \Lambda_{\text{QCD}}^2$ multiplied by a perturbative part. This can be extended to e^+e^- angularity to determine $\Omega_2^q(a)$ at nonzero a and to angularity in Higgs decay to determine corresponding corrections in the gluon channel. Following the convention of [87], the correction $\mathcal{O}(\Lambda_{\text{QCD}}^2/m_H^2)$ in Eq. (21) can be parameterized as $2M_{0,1}(a)\Omega_{1,1}(a)/m_H^2$, where $\Omega_{1,1}(a)$ is the correction appearing in the 2nd cumulant and $M_{0,1}(a)$ accounts for a perturbative part. Another way to study the subleading NP corrections is to take the difference between moments as in [88, 89] at two points in

a space

$$\begin{aligned} \Delta_{(a,a')} &= (1-a)\langle\tau_a^{\text{had}}\rangle - (1-a')\langle\tau_{a'}^{\text{had}}\rangle \\ &= (1-a)\langle\tau_a^{\text{pert}}\rangle - (1-a')\langle\tau_{a'}^{\text{pert}}\rangle + \mathcal{O}(\Lambda_{\text{QCD}}^2/m_H^2), \end{aligned} \quad (22)$$

where the leading correction Ω is cancelled in the second line and the subtracted moment $\Delta_{(a,a')}$ is sensitive to the subleading correction that can be expressed as a difference of the quantity $2(1-a)M_{0,1}(a)\Omega_{1,1}(a)/m_H^2$ at two points a and a' . By comparing experimental measurement and perturbative predictions one can determine the correction. The subtracted moment with angularity provides additional information different from that ob-

tained from thrust cumulant analysis hence, is a useful tool for extracting information on subleading NP corrections. Fig. 10 shows our perturbative predictions of Eq. (22) at NNLL' accuracies compared with Pythia simulations at parton and hadron levels for the gluon channel (left) and the quark channel (right). The Pythia results in the gluon channel show a notable difference between parton and hadron levels, while the difference in the quark channel is very small. This analysis can be done for different colliders such as Electron-Ion Collider [90] with DIS trust and angularity [44, 82, 83, 91] and determine NP corrections.

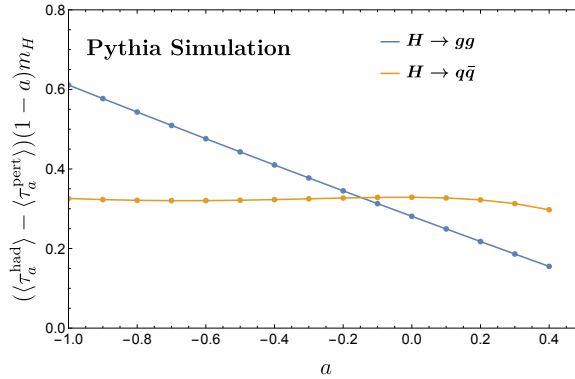


Fig. 9. Difference between $\langle\tau_a^{\text{had}}\rangle$ at hadron level and $\langle\tau_a^{\text{pert}}\rangle$ at parton level from Pythia simulation for gluon channel (blue) and for quark channel (orange).

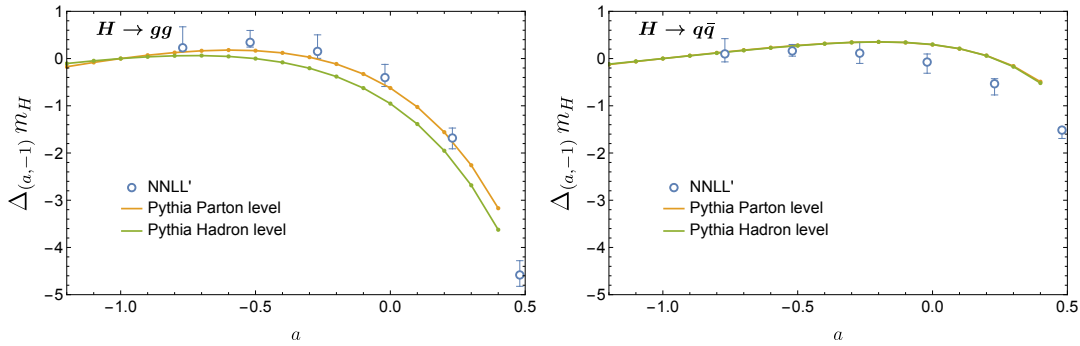


Fig. 10. Prediction of subtracted moment $\Delta_{(a,-1)}$ as a function of a from resummed results at NNLL' compared with Pythia simulations at parton and hadron levels for the quark channel (left) and for the gluon channel (right).

5 Conclusion

We present improved predictions of angularity distribution τ_a in hadronic decays of Higgs boson via effective operator $H \rightarrow gg$ that suffers from large perturbative uncertainties compared to the other contribution via Yukawa interaction $H \rightarrow q\bar{q}$. The distribution is

improved by resumming large logarithms of angularity at NNLL' accuracy in the framework of SCET and by matching the resummed results to the fixed-order result at NLO.

In order to achieve NNLL' accuracy, we independently determined a remaining ingredient, 2-loop constant of the gluon-jet function for angularity. We find

our values of the constant show reasonable agreement with the values in the literature. In the determination of the constant, there is significant contamination from subleading singular corrections slowly suppressed in the small τ_a limit. In order to estimate the correction, we use asymptotic forms in the small τ_a region and fit it to the nonsingular part of fixed-order result. The asymptotic form for $a \leq 0$ is $\sum_k \alpha_k \ln^k \tau_a$, which is one power-suppressed by the singular part, and for $0 < a \leq 1/2$ it has additional terms with fractional power $\sum_k \alpha_{1,k} \ln^k \tau_a / (\tau_a)^a$, which is conjectured from recoil corrections in one-loop soft function. The form in $a > 0$ has eight degrees of freedom and the fitting result is sensitive to noise hence, ill-posed. We found that it can be handled by adopting Tikhonov regularization that reduces the sensitivity to noise.

We also consider nonperturbative corrections in the

A SCET functions

Here, we summarize the functions appearing in the factorization in the gluon channel, and the tag g representing the gluon is implied implicitly. In Laplace space each function $G = \{C_t, C_S, \tilde{J}, \tilde{S}\}$ in Eq. (3) can be expressed as:

$$\begin{aligned}
G(L_G, \mu_G) &= \sum_{n=0}^{\infty} \left(\frac{\alpha_s(\mu_G)}{4\pi} \right)^n G^{(n)}(L_G) \\
G^{(0)}(L_G) &= 1 \\
G^{(1)}(L_G) &= [\Gamma_G^0 L_G^2 - \gamma_G^0 L_G + c_G^1] \\
G^{(2)}(L_G) &= \left[\frac{1}{2} (\Gamma_G^0)^2 L_G^4 - \Gamma_G^0 \left(\gamma_G^0 + \frac{2}{3} \beta_0 \right) L_G^3 \right. \\
&\quad \left. + \left(\Gamma_G^1 + \frac{1}{2} (\gamma_G^0)^2 + \gamma_G^0 \beta_0 + c_G^1 \Gamma_G^0 \right) L_G^2 - (\gamma_G^1 + c_G^1 \gamma_G^0 + 2c_G^1 \beta_0) L_G + c_G^2 \right],
\end{aligned} \tag{23}$$

where $\Gamma_G^n = -\frac{j_G \kappa_G}{2} \Gamma_n$. Γ_n , γ_G^n , c_G^n are coefficients of the universal cusp and non-cusp anomalous dimensions $\Gamma_{\text{cusp}}(\alpha_s)$ and $\gamma_G(\alpha_s)$ and of a constant term c_G in α_s expansion as

$$\begin{aligned}
\Gamma_{\text{cusp}}(\alpha_s) &= \sum_{n=0} \Gamma_n \left(\frac{\alpha_s}{4\pi} \right)^{n+1}, \\
\gamma_G(\alpha_s) &= \sum_{n=0} \gamma_G^n \left(\frac{\alpha_s}{4\pi} \right)^{n+1}, \\
c_G &= \sum_{n=1} c_G^n \left(\frac{\alpha_s}{4\pi} \right)^n,
\end{aligned} \tag{24}$$

where β_n and Γ_n are given in App. C and γ_G^n , and c_G^n are given in App. A.1 and App. A.2, respectively. The factors j_G and κ_G and $\log L_G$ are summarized in Table 4.

	C_t	C_S	\tilde{J}	\tilde{S}
j_G	1	1	$2 - a$	1
κ_G	0	2	$-2/(1 - a)$	$4/(1 - a)$
L_G	$\ln \frac{m_t}{\mu_{C_t}}$	$\ln \frac{im_H}{\mu_{C_S}}$	$\ln \left[\frac{m_H}{\mu_{\tilde{J}}} (\nu e^{\gamma_E})^{-1/j_{\tilde{J}}} \right]$	$\ln \left[\frac{m_H}{\mu_{\tilde{S}}} (\nu e^{\gamma_E})^{-1/j_{\tilde{S}}} \right]$

Table 4.

angularity. The corrections receive two contributions, one from the quark channel and the other from the gluon channel, and by using the value known for the quark in e^+e^- experiment, the gluon contribution can be determined from measurement in Higgs factories. Pythia simulation shows that the quark channel is comparable to the prediction of leading-power correction for the angularity, while the gluon channel is quite different from the prediction in a dependence and magnitude estimated from Casimir scaling. We also considered subtracted moment $\Delta_{(a,a')}$ defined by the difference between moments of τ_a at a and a' that mitigates the leading correction hence, it is sensitive to subleading corrections. The subtracted moment as a function of a is an independent direction from the cumulant analysis and provides additional information to the subleading correction.

Each term in Eq. (23) can be transformed into the momentum space by the inverse Laplace transformation as follows:

$$\begin{aligned}
1 &\rightarrow \delta(\tau) \\
-\ln \nu e^{\gamma_E} &\rightarrow \mathcal{L}_0(\tau) \\
\ln^2 \nu e^{\gamma_E} &\rightarrow 2\mathcal{L}_1(\tau) - \frac{\pi^2}{6}\delta(\tau) \\
-\ln^3 \nu e^{\gamma_E} &\rightarrow 3\mathcal{L}_2(\tau) - \frac{\pi^2}{2}\mathcal{L}_0(\tau) + 2\zeta_3\delta(\tau) \\
\ln^4 \nu e^{\gamma_E} &\rightarrow 4\mathcal{L}_3(\tau) - 2\pi^2\mathcal{L}_1(\tau) + 8\zeta_3\mathcal{L}_0(\tau) + \frac{\pi^4}{60}\delta(\tau),
\end{aligned} \tag{25}$$

where the distribution function $\mathcal{L}_n(\tau)$ is defined by

$$\mathcal{L}_n(\tau) = \begin{cases} \left[\frac{\ln^n(\tau)}{\tau} \right]_+ & n \geq 0, \\ \delta(\tau) & n = -1. \end{cases} \tag{26}$$

A.1 Non-cusp anomalous dimension

The anomalous dimension of the function G is defined by the Renormalization Group (RG) equation as

$$\mu \frac{d}{d\mu} G(\nu, \mu) = \gamma_G(\mu) G(\nu, \mu), \tag{27}$$

$$\gamma_G(\mu) = j_G \kappa_G \Gamma_{\text{cusp}}(\alpha_s) L_G + \gamma_G(\alpha_s) \tag{28}$$

From scale independence of the factorization in Eq. (3), we have a consistence relation:

$$\frac{2\beta(\alpha_s)}{\alpha_s} + 2\gamma_{C_t}(\alpha_s) + 2\gamma_{C_s}(\alpha_s) + 2\gamma_J(\alpha_s) + \gamma_S(\alpha_s) = 0 \tag{29}$$

where the first term is from the Born rate $\Gamma_B \propto \alpha_s^2$. The non-cusp anomalous dimensions of C_t [53–58] and C_S [61] are given by

$$\begin{aligned}
\gamma_{C_t}^0 &= 0, \quad \gamma_{C_t}^1 = -2\beta_1, \\
\gamma_{C_S}^0 &= 0, \quad \gamma_{C_S}^1 = \left(-\frac{118}{9} + 4\zeta_3 \right) C_A^2 + \left(-\frac{38}{9} + \frac{\pi^2}{3} \right) C_A \beta_0 + 2\beta_1,
\end{aligned} \tag{30}$$

The quark soft anomalous dimension is given in [42, 92], gluon soft anomalous dimension can be obtained from quark soft anomalous dimension by a Casimir scaling that is $C_F \rightarrow C_A$.

$$\gamma_S^0(a) = 0, \quad \gamma_S^1(a) = \frac{2}{1-a} [\gamma_1^{CA}(a) C_A^2 + \gamma_1^{nf}(a) C_A T_F n_f], \tag{31}$$

where we have made the a -dependence of the anomalous dimension explicit, and

$$\begin{aligned}
\gamma_1^{CA}(a) &= -\frac{808}{27} + \frac{11\pi^2}{9} + 28\zeta_3 - \Delta\gamma_1^{CA}(a), \\
\gamma_1^{nf}(a) &= \frac{224}{27} - \frac{4\pi^2}{9} - \Delta\gamma_1^{nf}(a),
\end{aligned} \tag{32}$$

where

$$\begin{aligned}
\Delta\gamma_1^{CA}(a) &= \int_0^1 dx \int_0^1 dy \frac{32x^2(1+xy+y^2)[x(1+y^2)+(x+y)(1+xy)]}{y(1-x^2)(x+y)^2(1+xy)^2} \ln \left[\frac{(x^a+xy)(x+x^a y)}{x^a(1+xy)(x+y)} \right], \\
\Delta\gamma_1^{nf}(a) &= \int_0^1 dx \int_0^1 dy \frac{64x^2(1+y^2)}{(1-x^2)(x+y)^2(1+xy)^2} \ln \left[\frac{(x^a+xy)(x+x^a y)}{x^a(1+xy)(x+y)} \right],
\end{aligned} \tag{33}$$

which vanish for thrust case $a=0$. Here we give numerical result at the values of a used in MC simulation.

a	-1.0	-0.75	-0.5	-0.25	0.0	0.25	0.5
γ_1^{CA}	1.0417	5.8649	9.8976	13.190	15.795	17.761	19.132
γ_1^{nf}	-0.9571	0.5284	1.8440	2.9751	3.9098	4.6398	5.1613

Then, we can obtain $\gamma_J(\alpha_s)$ is given by Eq. (29).

A.2 Constant term

Content terms in C_t [53–58] and C_S [61] are given by

$$\begin{aligned}
c_{C_t}^1 &= 11, \\
c_{C_t}^2 &= \frac{2777}{18} - \frac{67}{6}n_f, \\
c_{C_S}^1 &= C_A \frac{\pi^2}{6}, \\
c_{C_S}^2 &= C_A^2 \left(\frac{\pi^4}{72} - \frac{143\zeta_3}{9} + \frac{67\pi^2}{36} + \frac{5105}{162} \right) + C_F n_f \left(8\zeta_3 - \frac{67}{6} \right) + C_A n_f \left(-\frac{46\zeta_3}{9} - \frac{5\pi^2}{18} - \frac{916}{81} \right).
\end{aligned} \tag{34}$$

The constant term of quark soft functions is known to one-loop for generic values of a analytically [42], the two-loop constant is determined numerically for generic a in [62]. Gluon soft function can be obtained from quark soft function constant by a Casimir scaling that is $C_F \rightarrow C_A$. In Laplace space:

$$\begin{aligned}
c_S^1(a) &= -C_A \frac{\pi^2}{1-a}, \\
c_S^2(a) &= c_2^{CA}(a)C_A^2 + c_2^{nf}(a)C_A T_F n_f + \frac{\pi^4}{2(1-a)^2} C_A^2,
\end{aligned} \tag{35}$$

where

a	-1.0	-0.75	-0.5	-0.25	0.0	0.25	0.5
c_2^{CA}	-22.430	-29.170	-36.398	-44.962	-56.499	-74.717	-110.55
c_2^{nf}	27.315	28.896	31.589	36.016	43.391	56.501	83.670

One-loop constant of gluon jet function [93, 94] in Laplace space is given by

$$\begin{aligned}
c_J^1(a) &= c_J^1(a) + \frac{\Gamma_J^0(a)}{(2-a)^2} \frac{\pi^2}{6} \\
&= \frac{2}{1-a/2} \left[C_A \left((1-a) \left(\frac{67}{18} - \frac{\pi^2}{3} \right) - \frac{\pi^2}{6} \frac{(1-a/2)^2 - 1}{1-a} - f_1(a) \right) - T_F n_f \left(\frac{20-23a}{18} - f_2(a) \right) \right],
\end{aligned} \tag{36}$$

where

$$\begin{aligned}
f_1(a) &= \int_0^1 dx \frac{(1-x(1-x))^2}{x(1-x)} \ln[x^{1-a} + (1-x)^{1-a}] \\
f_2(a) &= \int_0^1 dx (2x(1-x) - 1) \ln[x^{1-a} + (1-x)^{1-a}].
\end{aligned} \tag{37}$$

Note that in Eq. (36) the minus sign of $\pi^2/6$ term is opposite in Eq. (11) of Ref. [94], which we think is a typo since following their recipe gives the minus and our numerical result for c_J^1 is consistent with the minus.

The two-loop constant is numerically obtained and is given in Table 3.

B Resummation formula

The large logs in C_t , C_S , \tilde{J} and \tilde{S} can be resummed by the RG evolution starting from natural scales, in which the logs are small, to an arbitrary scale μ . The solution of RGE in Eq. (27) shares the following structure:

$$G^{\text{res}}(\nu, \mu) = G(\nu, \mu_G) e^{K_G(\mu_G, \mu) + j_G \eta_G(\mu_G, \mu) L_G}, \tag{38}$$

where K_G and η_G are integration of $\gamma_G(\mu)$ in Eq. (28) from μ_G to μ

$$\int_{\mu_G}^{\mu} \frac{d\mu'}{\mu'} \gamma_G(\mu') = j_G \kappa_G \int_{\mu_G}^{\mu} \frac{d\mu'}{\mu'} \Gamma_{\text{cusp}}(\alpha_s) [-\ln(\mu'/\mu_G) + L_G(\mu_G)] + \int_{\mu_G}^{\mu} \frac{d\mu'}{\mu'} \gamma_G(\alpha_s). \tag{39}$$

After replacing $\frac{d\mu'}{\mu'}$ by $d\alpha_s/\beta(\alpha_s)$, we define three integrals as

$$\begin{aligned} K_\Gamma(\mu_G, \mu) &= \int_{\alpha_s(\mu_G)}^{\alpha_s(\mu)} \frac{d\alpha_s}{\beta(\alpha_s)} \Gamma_{\text{cusp}}(\alpha_s) \int_{\alpha_s(\mu_G)}^{\alpha_s} \frac{d\alpha'_s}{\beta(\alpha'_s)}, \\ \eta_\Gamma(\mu_G, \mu) &= \int_{\alpha_s(\mu_G)}^{\alpha_s(\mu)} \frac{d\alpha_s}{\beta(\alpha_s)} \Gamma_{\text{cusp}}(\alpha_s), \\ K_{\gamma_G}(\mu_G, \mu) &= \int_{\alpha_s(\mu_G)}^{\alpha_s(\mu)} \frac{d\alpha_s}{\beta(\alpha_s)} \gamma_G(\alpha_s). \end{aligned} \quad (40)$$

In App. C we give results of integration done order by order in α_s . We define K_G and η_G as

$$\begin{aligned} K_G(\mu_G, \mu) &= -j_G \kappa_G K_\Gamma(\mu_G, \mu) + K_{\gamma_G}(\mu_G, \mu), \\ \eta_G(\mu_G, \mu) &= \kappa_G \eta_\Gamma(\mu_G, \mu). \end{aligned} \quad (41)$$

Now we review conversion of resummed results in Laplace space back to momentum space by the inverse Laplace transformation

$$\mathcal{L}^{-1}\{f(\nu)\} = \frac{1}{2\pi i} \int_{\gamma-i\infty}^{\gamma+i\infty} d\nu e^{\nu\tau_a} f(\nu) \quad (42)$$

In order to make the inverse integration simple, we replace all ν -dependent log by derivative operators as $L_G \rightarrow \partial_{\eta_G}/j_G$ in the fixed-order function $G(\nu, \mu)$ in Eq. (23) and rewrite the resummed function in Eq. (38) as

$$G^{\text{res}}(\nu, \mu) = g(\partial_{\eta_G}) e^{K_G(\mu_G, \mu) + j_G \eta_G(\mu_G, \mu) L_G}, \quad (43)$$

where $g(\partial_{\eta_G}) = G(\nu, \mu)|_{L_G \rightarrow \partial_{\eta_G}/j_G}$. One finds Eq. (43) is equivalent to Eq. (38).

At $\mathcal{O}(\alpha_s)$ we have the fix-order function $g(\partial_{\eta_G})$:

$$g(\partial_{\eta_G}) = 1 + \frac{\alpha_s(\mu)}{4\pi} \left[-\kappa_G \frac{\Gamma_0}{2j_G} \partial_{\eta_G}^2 - \frac{\gamma_0^G}{j_G} \partial_{\eta_G} + c_G^1 \right], \quad (44)$$

Using an identity of inverse transformation

$$\mathcal{L}^{-1}\{\nu^{-\eta_G}\} = \frac{\tau_a^{\eta_G-1}}{\Gamma(\eta_G)}, \quad (45)$$

Eq. (43) turns into the resummed function in momentum space as

$$G^{\text{res}}(\tau_a, \mu) = \frac{e^{K_G}}{\tau_a} g(\partial_{\eta_G}) \frac{e^{j_G \eta_G L_G(\tau_a)}}{\Gamma(\eta_G)}, \quad (46)$$

where the logarithm in τ_a is defined by

$$L_G(\tau_a) = \ln \left[\frac{Q}{\mu_G} (\tau_a e^{-\gamma_E})^{1/j_G} \right], \quad G = \{S, J\}. \quad (47)$$

The resummed distribution is product of jet, and soft functions expressed in a form of Eq. (43) then, η_G in Eq. (45) is replaced by the sum $\Omega = \eta_S + 2\eta_J$. Finally, we obtain:

$$\begin{aligned} \frac{1}{\Gamma_B} \frac{d\Gamma^{\text{res}}}{d\tau_a} &= \frac{\alpha_s(\mu)^2}{\alpha_s(m_H)^2} |C_t(m_t, \mu_{C_t})|^2 |C_s(m_H, \mu_H)|^2 j^2(\partial_{\eta_J}) s(\partial_{\eta_S}) \\ &\times e^{\kappa(\{\mu_i\}, \mu)} \left(\frac{m_t}{\mu_{C_t}} \right)^{2\eta_{C_t}(\mu_{C_t}, \mu)} \left| \left(\frac{im_H}{\mu_{C_s}} \right)^{\eta_{C_s}(\mu_{C_s}, \mu)} \right|^2 \left(\frac{m_H}{\mu_J} \right)^{2j_J \eta_J(\mu_J, \mu)} \left(\frac{m_H}{\mu_S} \right)^{j_S \eta_S(\mu_S, \mu)} \\ &\times \frac{\tau_a^{-1+\Omega}}{\Gamma(\Omega)} e^{-\gamma_E \Omega}, \end{aligned} \quad (48)$$

where

$$\kappa(\{\mu_i\}, \mu) = 2K_{C_t}(\mu_{C_t}, \mu) + K_{C_s}(\mu_{C_s}, \mu) + K_{C_s}^*(\mu_{C_s}, \mu) + 2K_J(\mu_J, \mu) + K_S(\mu_S, \mu). \quad (49)$$

In the numerical calculation, we set $\mu_{C_t} = \mu_{C_S}$ to be the hard scale μ_H and vary them at the same time for a scale variation. By shifting the derivative by $L_G(\tau_a)$ all the exponents in Eq. (46) can be moved in the front as

$$G^{\text{res}}(\tau_a, \mu) = \frac{e^{K_G + j_G \eta_G L_G(\tau_a)}}{\tau_a} g(\partial_\Omega + j_G L_G(\tau_a)) \frac{1}{\Gamma(\Omega)}. \quad (50)$$

The operators $[\partial_\Omega + j_G L_G(\tau_a)]^n$ turns into poly-logarithms

$$\begin{aligned} [\partial_\Omega + j_G L_G(\tau_a)] \frac{1}{\Gamma(\Omega)} &= \psi_G(\Omega) \frac{1}{\Gamma(\Omega)}, \\ [\partial_\Omega + j_G L_G(\tau_a)]^2 \frac{1}{\Gamma(\Omega)} &= \{\psi_G^2(\Omega) - \psi^{(1)}(\Omega)\} \frac{1}{\Gamma(\Omega)}, \\ [\partial_\Omega + j_G L_G(\tau_a)]^3 \frac{1}{\Gamma(\Omega)} &= \{\psi_G^3(\Omega) - 3\psi_G \psi^{(1)}(\Omega) - \psi^{(2)}(\Omega)\} \frac{1}{\Gamma(\Omega)}, \\ [\partial_\Omega + j_G L_G(\tau_a)]^4 \frac{1}{\Gamma(\Omega)} &= \{\psi_G^4(\Omega) - 6\psi_G^2 \psi^{(1)}(\Omega) - 4\psi_G \psi^{(2)}(\Omega) + 3(\psi^{(1)}(\Omega))^2 - \psi^{(3)}(\Omega)\} \frac{1}{\Gamma(\Omega)}, \end{aligned} \quad (51)$$

where

$$\begin{aligned} \psi(\Omega) &= \Gamma'(\Omega)/\Gamma(\Omega), \\ \psi_G(\Omega) &= -\psi(\Omega) + j_G L_G(\tau_a), \\ \psi^{(n)}(\Omega) &= \frac{d^n \psi(\Omega)}{d\Omega^n}. \end{aligned} \quad (52)$$

We would like to note that operators in crossing terms like $\alpha_s^2 s_1 j_1$ are not simply the square of the second line in Eq. (51) and need to be carefully expanded as

$$\begin{aligned} &[\partial_\Omega + j_{G1} L_{G1}(\tau_a)]^2 [\partial_\Omega + j_{G2} L_{G2}(\tau_a)]^2 \frac{1}{\Gamma(\Omega)} \\ &= \{\psi_{G1}^2 \psi_{G2}^2 - (\psi_{G1}^2 + 4\psi_{G1} \psi_{G2} + \psi_{G2}^2) \psi^{(1)}(\Omega) - (2\psi_{G1} + 2\psi_{G2}) \psi^{(2)}(\Omega) + 3(\psi^{(1)}(\Omega))^2 - \psi^{(3)}(\Omega)\} \frac{1}{\Gamma(\Omega)} \end{aligned} \quad (53)$$

Our final form of the resummed result is given by

$$\begin{aligned} \frac{1}{\Gamma_0} \frac{d\Gamma^{\text{res}}}{d\tau_a} &= \frac{\alpha_s(\mu)^2}{\alpha_s(m_H)^2} |C_t(m_t, \mu_{C_t})|^2 |C_s(m_H, \mu_{C_S})|^2 e^{\kappa(\{\mu_i\}, \mu)} \\ &\times \tau_a^{-1+\Omega} e^{-\gamma_E \Omega} \left(\frac{m_t}{\mu_{C_t}}\right)^{2\eta_{C_t}(\mu_{C_t}, \mu)} \left|\left(\frac{i m_H}{\mu_{C_S}}\right)^{\eta_{C_S}(\mu_{C_S}, \mu)}\right|^2 \left(\frac{m_H}{\mu_J}\right)^{2j_J \eta_J(\mu_J, \mu)} \left(\frac{m_H}{\mu_S}\right)^{j_S \eta_S(\mu_S, \mu)} \\ &\times \left[j^2 \left(\partial_\Omega + j_J L_J(\tau_a), \mu_J \right) s \left(\partial_\Omega + j_S L_S(\tau_a), \mu_S \right) \right] \frac{1}{\Gamma(\Omega)}. \end{aligned} \quad (54)$$

C Cusp anomalous dimensions and related integral

Here, we summarize the coefficient of cusp-anomalous and beta function and integrals defined in Eq. (40) in the resummation.

To the NNLL order, we need up to three-loop cusp anomalous dimension for gluon [95, 96], which is related to quark channel by the ratio of the eigenvalues C_i of the quadratic Casimir operators up to 3-loop [95]: $\frac{\Gamma_{\text{cusp}}^g(\alpha_s)}{C_F} = \frac{\Gamma_{\text{cusp}}^g(\alpha_s)}{C_A}$. Note that it is different from the soft function where all the C_F are replaced by C_A . Here we give cusp anomalous dimension for gluon without subscript g .

$$\begin{aligned} \Gamma_0 &= 4C_A \\ \Gamma_1 &= \Gamma_0 \left[\left(\frac{67}{9} - \frac{\pi^2}{3} \right) C_A - \frac{20}{9} T_F n_f \right] \\ \Gamma_2 &= \Gamma_0 \left[\left(\frac{245}{6} - \frac{134\pi^2}{27} + \frac{11\pi^4}{45} + \frac{22\zeta_3}{3} \right) C_A^2 + \left(-\frac{418}{27} + \frac{40\pi^2}{27} - \frac{56\zeta_3}{3} \right) C_A T_F n_f + \left(-\frac{55}{3} + 16\zeta_3 \right) C_F T_F n_f - \frac{16}{27} T_F^2 n_f^2 \right] \end{aligned} \quad (55a)$$

The beta function expanded in powers of α_s is given by

$$\beta(\alpha_s) = \mu \frac{d\alpha_s(\mu)}{d\mu} = -2\alpha_s \sum_{n=0}^{\infty} \beta_n \left(\frac{\alpha_s}{4\pi}\right)^{n+1} \quad (56)$$

The beta-function coefficients [97, 98] are

$$\begin{aligned} \beta_0 &= \frac{11}{3} C_A - \frac{4}{3} T_F n_f, \\ \beta_1 &= \frac{34}{3} C_A^2 - \left(\frac{20}{3} C_A + 4C_F\right) T_F n_f, \\ \beta_2 &= \frac{2857}{54} C_A^3 + \left(C_F^2 - \frac{205}{18} C_F C_A - \frac{1415}{54} C_A^2\right) 2T_F n_f + \left(\frac{11}{9} C_F + \frac{79}{54} C_A\right) 4T_F^2 n_f^2. \end{aligned} \quad (57)$$

An expansion of Eq. (40) in powers of α_s is

$$\begin{aligned} K_\Gamma(\mu_0, \mu) &= -\frac{\Gamma_0}{4\beta_0^2} \left\{ \frac{4\pi}{\alpha_s(\mu_0)} \left(1 - \frac{1}{r} - \ln r\right) + \left(\frac{\Gamma_1}{\Gamma_0} - \frac{\beta_1}{\beta_0}\right) (1 - r + \ln r) + \frac{\beta_1}{2\beta_0} \ln^2 r \right. \\ &\quad \left. + \frac{\alpha_s(\mu_0)}{4\pi} \left[\left(\frac{\beta_1^2}{\beta_0^2} - \frac{\beta_2}{\beta_0}\right) \left(\frac{1-r^2}{2} + \ln r\right) + \left(\frac{\beta_1\Gamma_1}{\beta_0\Gamma_0} - \frac{\beta_1^2}{\beta_0^2}\right) (1 - r + r \ln r) - \left(\frac{\Gamma_2}{\Gamma_0} - \frac{\beta_1\Gamma_1}{\beta_0\Gamma_0}\right) \frac{(1-r)^2}{2} \right] \right\}, \\ \eta_\Gamma(\mu_0, \mu) &= -\frac{\Gamma_0}{2\beta_0} \left[\ln r + \frac{\alpha_s(\mu_0)}{4\pi} \left(\frac{\Gamma_1}{\Gamma_0} - \frac{\beta_1}{\beta_0}\right) (r-1) + \frac{\alpha_s^2(\mu_0)}{16\pi^2} \left(\frac{\Gamma_2}{\Gamma_0} - \frac{\beta_1\Gamma_1}{\beta_0\Gamma_0} + \frac{\beta_1^2}{\beta_0^2} - \frac{\beta_2}{\beta_0}\right) \frac{r^2-1}{2} \right], \\ K_\gamma(\mu_0, \mu) &= -\frac{\gamma_0}{2\beta_0} \left[\ln r + \frac{\alpha_s(\mu_0)}{4\pi} \left(\frac{\gamma_1}{\gamma_0} - \frac{\beta_1}{\beta_0}\right) (r-1) \right]. \end{aligned} \quad (58)$$

Here, $r = \alpha_s(\mu)/\alpha_s(\mu_0)$. Solving the beta function to three-loop order gives the running coupling expressed by

$$\frac{1}{\alpha_s(\mu)} = \frac{X}{\alpha_s(\mu_0)} + \frac{\beta_1}{4\pi\beta_0} \ln X + \frac{\alpha_s(\mu_0)}{16\pi^2} \left[\frac{\beta_2}{\beta_0} \left(1 - \frac{1}{X}\right) + \frac{\beta_1^2}{\beta_0^2} \left(\frac{\ln X}{X} + \frac{1}{X} - 1\right) \right], \quad (59)$$

where $X \equiv 1 + \alpha_s(\mu_0)\beta_0 \ln(\mu/\mu_0)/(2\pi)$. In our numerical calculations, we take the full NNLL results in Eq. (58) for $K_{\Gamma,\gamma}, \eta_\Gamma$ and in Eq. (59).

D Tikhonov method

For a known matrix A and vector \mathbf{b} , a least-square method is to find a vector \mathbf{x} such that it minimizes the square residuals $|\mathbf{A}\mathbf{x} - \mathbf{b}|^2$, where $|\cdot|^2$ is the vector squared. In our problem, \mathbf{b}_i is the value of remainder function at i_{th} bin, \mathbf{x}_j is j_{th} parameter in the fit function, and A_{ij} is the value of j_{th} term of fit function at i_{th} bin. $\hat{\mathbf{x}} = (A^T A)^{-1} A^T \mathbf{b}$ is the solution to zero gradient of the square residuals. However, in some cases, matrix $A^T A$ is nearly singular and sensitive to small changes in data like noise. In those cases regression is said to be ill-posed, and generally regularization helps improve the result. We adopt Tikhonov regularization [76], in which a regularization term is included in the squared residuals $|\mathbf{A}\mathbf{x} - \mathbf{b}|^2 + \lambda |\Gamma \mathbf{x}|^2$, where λ is a regularization parameter and Γ is a Tikhonov matrix. With the introduction of the regularization term, the solution to zero gradient is $\hat{\mathbf{x}} = (A^T A + \lambda \Gamma^T \Gamma)^{-1} A^T \mathbf{b}$, where $\lambda \Gamma^T \Gamma$ tames the singu-

larity of $A^T A$.

The regularization depends on the choice of regularization parameter λ and Tikhonov matrix Γ . We take the identity matrix for Γ in our analysis. We also test with discrete first- and second-order derivative matrices that give $\Gamma \mathbf{x} = (x_2 - x_1, \dots, x_n - x_{n-1})^T$ and $(x_3 - 2x_2 + x_1, \dots, x_n + 2x_{n-1} - x_{n-2})^T$ and they essentially give consistent result with that with identity matrix. The regularization parameter should be assigned carefully, a tiny value cannot tame the singularity, while a too large value would distort the feature of the remainder function. We select the value of parameter that gives a robust fit result against variations of upper and lower bounds of the fit region. We find that for non-positive a cases, the value of the regularization parameter is small $\lambda = 10^{-4}$, which essentially equivalent to ordinary least-square, i.e., $\lambda = 0$. For positive a , the parameter is larger $\lambda = 10^3(10^1)$ for $a = 0.25$ and $\lambda = 10^4(10^3)$ for $a = 0.5$ in the quark (gluon) channel.

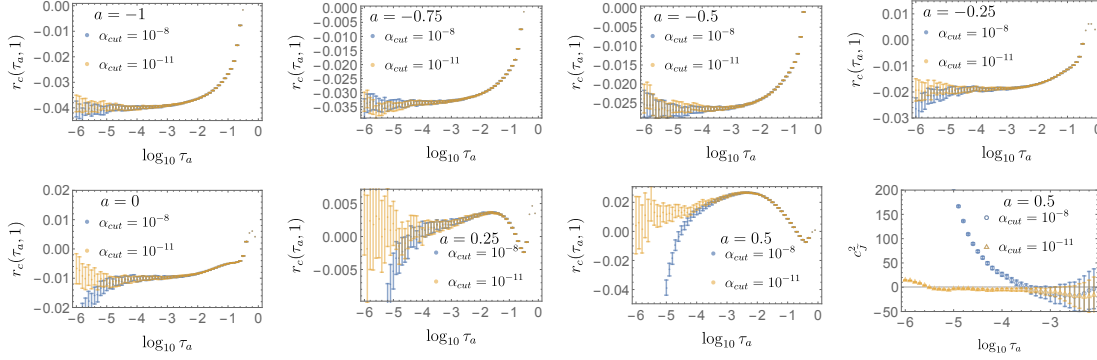


Fig. 11. NLO remainder functions for $\alpha_{\text{cut}} = 10^{-11}$ (blue) and for 10^{-8} (yellow) at seven different values of a . The last plot shows prediction of 2-loop constant c_J^2 as a function of lower bound τ_a^{low} for $\alpha_{\text{cut}} = 10^{-11}$ and for 10^{-8} .

E Cutoff effect

We explore the effect of cutoff α_{cut} in the quark channel by comparing our standard value $\alpha_{\text{cut}} = 10^{-11}$ and larger value 10^{-8} as shown in Fig. 11. Their differences are hardly visible in $a < 0$ in given ranges of τ_a and become visible in $a \geq 0$. The last plot in Fig. 11 shows the constant c_J^2 as a function of τ_a^{low} at $a = 0.5$. While the value of constant stays still in the domain $\log_{10} \tau_a^{\text{low}} \in \{-4.5, -2.6\}$ for $\alpha_{\text{cut}} = 10^{-11}$, for $\alpha_{\text{cut}} = 10^{-8}$ it begins to change around $\log_{10} \tau_a^{\text{low}} = -3.5$ and below.

This implies that the fit regions for $\alpha_{\text{cut}} = 10^{-11}$ in Fig. 5 is insensitive to the cutoff effect. For $\alpha_{\text{cut}} = 10^{-8}$ we use same criteria and obtained $c_J^2 = -55.90 \pm 1.84$ at $a = 0.25$ and -10.33 ± 11.44 at $a = 0.5$, which are consistent with the values in Table 2.

Fig. 12 shows the cutoff effect in the gluon channel as a function of τ_a^{low} with $\log_{10} \tau_a^{\text{high}} = -1.4 + 0.4(1+a)$ held fixed. Similar to the quark channel, larger a values tend to suffer from greater cutoff effect c_J^2 . Using the results, our fit regions are selected to avoid the cutoff effect as described in the main body of the paper.

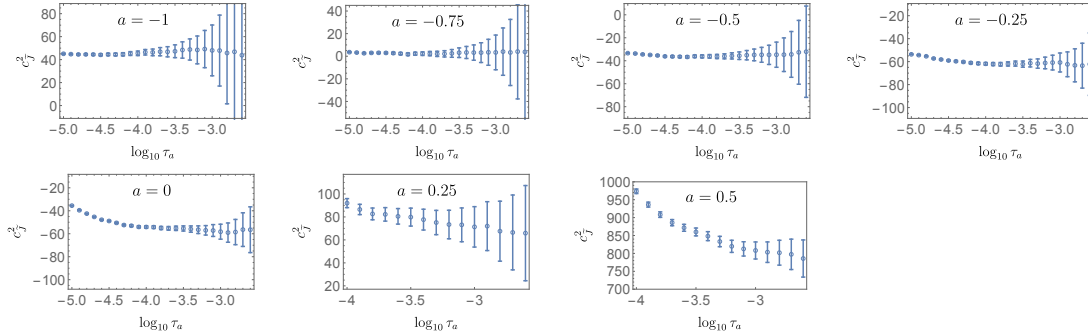


Fig. 12. two-loop constant c_J^2 as a function of lower bound τ_a^{low} with fixed-upper bound $\log_{10} \tau_a^{\text{high}} = -1.4 + 0.4(1+a)$ at $\alpha_{\text{cut}} = 10^{-8}$

References

- 1 ATLAS collaboration, *Phys. Lett. B*, **716**: 1 (2012)
- 2 CMS collaboration, *Phys. Lett. B*, **716**: 30 (2012)
- 3 CMS collaboration, *Phys. Rev. Lett.*, **120**: 231801 (2018)
- 4 ATLAS collaboration, *Phys. Lett. B*, **784**: 173 (2018)
- 5 ATLAS collaboration, *Phys. Lett. B*, **786**: 59 (2018)
- 6 CMS collaboration, *Phys. Rev. Lett.*, **121**: 121801 (2018)
- 7 CMS collaboration, *Sensitivity projections for Higgs boson properties measurements at the HL-LHC, CMS-PAS-FTR-18-011*.
- 8 J. Gao, *JHEP*, **02**: 094 (2014)
- 9 Y. Soreq, H.X. Zhu and J. Zupan, *JHEP*, **12**: 045 (2016)
- 10 F. Bishara, U. Haisch, P.F. Monni et al, *Phys. Rev. Lett.*, **118**: 121801 (2017)
- 11 G.T. Bodwin, F. Petriello, S. Stoynev et al, *Phys. Rev. D*, **88**: 053003 (2013)
- 12 A.L. Kagan, G. Perez, F. Petriello et al, *Phys. Rev. Lett.*, **114**: 101802 (2015)
- 13 Y. Zhou, *Phys. Rev. D*, **93**: 013019 (2016)
- 14 M. König and M. Neubert, *JHEP*, **08**: 012 (2015)
- 15 G. Perez, Y. Soreq, E. Stamou et al, *Phys. Rev. D*, **93**: 013001 (2016)
- 16 A.S. Chisholm, S. Kuttimalai, K. Nikolopoulos et al, *Eur. Phys. J. C*, **76**: 501 (2016)
- 17 F. Goertz, A. Papaefstathiou, L.L. Yang et al, *JHEP*, **06**: 016 (2013)
- 18 CMS collaboration, *Phys. Rev. Lett.*, **122**: 121803 (2019)
- 19 CMS collaboration, *Prospects for HH measurements at the HL-LHC, CMS-PAS-FTR-18-019*.
- 20 ATLAS collaboration, *JHEP*, **11**: 040 (2018)

- 21 T. Behnke, J.E. Brau, B. Foster et al, eds., arxiv: [1306.6327](#).
- 22 CEPC STUDY GROUP collaboration, arxiv: [1811.10545](#).
- 23 P. Lebrun, L. Linssen, A. Lucaci-Timoce et al, arxiv: [1209.2543](#).
- 24 TLEP DESIGN STUDY WORKING GROUP collaboration, *JHEP*, **01**: 164 (2014)
- 25 J. Gao, *JHEP*, **01**: 038 (2018)
- 26 J. Gao, Y. Gong, W.-L. Ju et al, *JHEP*, **03**: 030 (2019)
- 27 M.-X. Luo, V. Shtabovenko, T.-Z. Yang et al, *JHEP*, **06**: 037 (2019)
- 28 J. Gao, V. Shtabovenko and T.-Z. Yang, *JHEP*, **02**: 210 (2021)
- 29 G. Coloretti, A. Gehrmann-De Ridder and C.T. Preuss, *JHEP*, **06**: 009 (2022)
- 30 A. Gehrmann-De Ridder, C.T. Preuss and C. Williams, arxiv: [2310.09354](#).
- 31 J. Mo, F.J. Tackmann and W.J. Waalewijn, *Eur. Phys. J. C*, **77**: 770 (2017)
- 32 S. Alioli, A. Broggio, A. Gavardi et al, *JHEP*, **04**: 254 (2021)
- 33 W.-L. Ju, Y. Xu, L.L. Yang et al, *Phys. Rev. D*, **107**: 114034 (2023)
- 34 B. Yan and C. Lee, *Probing light quark Yukawa couplings through jet angularities in Higgs boson decay*, in *The 2022 International Workshop on the High Energy Circular Electron Positron Collider*.
- 35 M. van Beekveld, M. Dasgupta, B.K. El-Menoufi et al, *JHEP*, **05**: 093 (2024)
- 36 C.W. Bauer, S. Fleming and M.E. Luke, *Phys. Rev. D*, **63**: 014006 (2000)
- 37 C.W. Bauer, S. Fleming, D. Pirjol et al, *Phys. Rev. D*, **63**: 114020 (2001)
- 38 C.W. Bauer and I.W. Stewart, *Phys. Lett. B*, **516**: 134 (2001)
- 39 C.W. Bauer, D. Pirjol and I.W. Stewart, *Phys. Rev. D*, **65**: 054022 (2002)
- 40 C.W. Bauer, S. Fleming, D. Pirjol et al, *Phys. Rev. D*, **66**: 014017 (2002)
- 41 C.W. Bauer, S.P. Fleming, C. Lee et al, *Phys. Rev. D*, **78**: 034027 (2008)
- 42 A. Hornig, C. Lee and G. Ovanesyanyan, *JHEP*, **05**: 122 (2009)
- 43 G. Bell, A. Hornig, C. Lee et al, *JHEP*, **01**: 147 (2019)
- 44 J. Zhu, D. Kang and T. Maji, *JHEP*, **11**: 026 (2021)
- 45 A. Budhraj, A. Jain and M. Procura, *JHEP*, **08**: 144 (2019)
- 46 T. Becher, G. Bell and M. Neubert, *Phys. Lett. B*, **704** (2011) 276
- 47 T. Becher and G. Bell, *JHEP*, **11**: 126 (2012)
- 48 A.J. Larkoski, D. Neill and J. Thaler, *JHEP*, **04**: 017 (2014)
- 49 P. Bijl, S. Niedenzu and W.J. Waalewijn, arxiv: [2307.02521](#).
- 50 M. Procura, W.J. Waalewijn and L. Zeune, *JHEP*, **10**: 098 (2018)
- 51 M. Beneke, A.P. Chapovsky, M. Diehl et al, *Nucl. Phys. B*, **643**: 431 (2002)
- 52 M. Beneke and T. Feldmann, *Phys. Lett. B*, **553**: 267 (2003)
- 53 T. Inami, T. Kubota and Y. Okada, *Z. Phys. C*, **18**: 69 (1983) .
- 54 A. Djouadi, J. Kalinowski and P.M. Zerwas, *Z. Phys. C*, **54**: 255 (1992) .
- 55 K.G. Chetyrkin, B.A. Kniehl and M. Steinhauser, *Phys. Rev. Lett.* , **79**: 353 (1997)
- 56 K.G. Chetyrkin, B.A. Kniehl and M. Steinhauser, *Nucl. Phys. B*, **510**: 61 (1998)
- 57 K.G. Chetyrkin, J.H. Kuhn and C. Sturm, *Nucl. Phys. B*, **744**: 121 (2006)
- 58 P.A. Baikov, K.G. Chetyrkin and J.H. Kühn, *Phys. Rev. Lett.* , **118**: 082002 (2017)
- 59 M.D. Schwartz, *Phys. Rev. D*, **77**: 014026 (2008)
- 60 T. Becher and M.D. Schwartz, *JHEP*, **07**: 034 (2008)
- 61 T. Gehrmann, E.W.N. Glover, T. Huber et al, *JHEP*, **06**: 094 (2010)
- 62 G. Bell, R. Rahn and J. Talbert, *JHEP*, **09**: 015 (2020)
- 63 G. Bell, R. Rahn and J. Talbert, *JHEP*, **07**: 101 (2019)
- 64 K.M. Brune, *Automation of jet function calculations in Soft-Collinear Effective theory*, Ph.D. thesis, Siegen U., 2022. dx.doi.org/10.25819/ubsi/10228.
- 65 Z. Ligeti, I.W. Stewart and F.J. Tackmann, *Phys. Rev. D*, **78**: 114014 (2008)
- 66 R. Abbate, M. Fickinger, A.H. Hoang et al, *Phys. Rev. D*, **83**: 074021 (2011)
- 67 T. Becher, M. Neubert and B.D. Pecjak, *JHEP*, **01**: 076 (2007)
- 68 T. Becher and M. Neubert, *Phys. Rev. Lett.* , **97**: 082001 (2006)
- 69 A.H. Hoang and S. Kluth, arxiv: [0806.3852](#).
- 70 S. Catani and M.H. Seymour, *Nucl. Phys. B*, **485**: 291 (1997)
- 71 S.G. Gorishnii, A.L. Kataev, S.A. Larin et al, *Mod. Phys. Lett. A*, **5**: 2703 (1990) .
- 72 OPENLOOPS 2 collaboration, *Eur. Phys. J. C*, **79**: 866 (2019)
- 73 A. van Hameren, *Comput. Phys. Commun.* , **182**: 2427 (2011)
- 74 G. Ossola, C.G. Papadopoulos and R. Pittau, *JHEP*, **03**: 042 (2008)
- 75 T. Hahn, *Comput. Phys. Commun.* , **168**: 78 (2005)
- 76 A.N. Tikhonov, *Doklady akademii nauk*, , vol. 151, pp. 501–504, Russian Academy of Sciences, 1963.
- 77 Z. Nagy and Z. Trocsanyi, *Phys. Rev. D*, **59**: 014020 (1999)
- 78 Z. Nagy, *Phys. Rev. D*, **68**: 094002 (2003)
- 79 T. Gleisberg and F. Krauss, *Eur. Phys. J. C*, **53**: 501 (2008)
- 80 G. Bell, K. Brune, G. Das et al, *SciPost Phys. Proc.* , **7**: 021 (2022)
- 81 C.F. Berger, C. Marcantonini, I.W. Stewart et al, *JHEP*, **04**: 092 (2011)
- 82 D. Kang, C. Lee and I.W. Stewart, *Phys. Rev. D*, **88**: 054004 (2013)
- 83 D. Kang, C. Lee and I.W. Stewart, *JHEP*, **11**: 132 (2014)
- 84 C. Lee and G.F. Sterman, *Phys. Rev. D*, **75**: 014022 (2007)
- 85 A.H. Hoang and I.W. Stewart, *Phys. Lett. B*, **660**: 483 (2008)
- 86 C.F. Berger and G.F. Sterman, *JHEP*, **09**: 058 (2003)
- 87 R. Abbate, M. Fickinger, A.H. Hoang et al, *Phys. Rev. D*, **86**: 094002 (2012)
- 88 Y.-T. Chien, D. Kang, K. Lee et al, *Phys. Rev. D*, **100**: 074030 (2019)
- 89 D. Kang, Y. Makris and T. Mehen, *JHEP*, **09**: 055 (2018)
- 90 R. Abdul Khalek et al., arxiv: [2103.05419](#).
- 91 Z. Chu, Y. Wang, J.-H. Ee et al, *JHEP*, **06**: 111 (2022)
- 92 G. Bell, R. Rahn and J. Talbert, *Nucl. Phys. B*, **936**: 520 (2018)
- 93 S.D. Ellis, C.K. Vermilion, J.R. Walsh et al, *JHEP*, **11**: 101 (2010)
- 94 A. Hornig, Y. Makris and T. Mehen, *JHEP*, **04**: 097 (2016)
- 95 S. Moch, J.A.M. Vermaseren and A. Vogt, *Nucl. Phys. B*, **688**: 101 (2004)
- 96 G.P. Korchemsky and A.V. Radyushkin, *Nucl. Phys. B*, **283**: 342 (1987) .
- 97 S.A. Larin and J.A.M. Vermaseren, *Phys. Lett. B*, **303**: 334 (1993)
- 98 O.V. Tarasov, A.A. Vladimirov and A.Y. Zharkov, *Phys. Lett. B*, **93**: 429 (1980) .